Targeting and functional mechanisms of the cytokinesis-related F-BAR protein Hof1 during the cell cycle

Younghoon Oh[a], Jennifer Schreiter[a], Ryuichi Nishihama[b,*], Carsten Wloka[a,c], and Erfei Bi[a]
[a]Department of Cell and Developmental Biology, Perelman School of Medicine, University of Pennsylvania, Philadelphia, PA 19104; [b]Department of Genetics, Stanford University School of Medicine, Stanford, CA 94305; [c]Institut für Biologie, Freie Universität Berlin, 14195 Berlin, Germany

ABSTRACT **F-BAR proteins are membrane-associated proteins believed to link the plasma membrane to the actin cytoskeleton in cellular processes such as cytokinesis and endocytosis. In the budding yeast *Saccharomyces cerevisiae*, the F-BAR protein Hof1 localizes to the division site in a complex pattern during the cell cycle and plays an important role in cytokinesis. However, the mechanisms underlying its localization and function are poorly understood. Here we show that Hof1 contains three distinct targeting domains that contribute to cytokinesis differentially. The N-terminal half of Hof1 localizes to the bud neck and the sites of polarized growth during the cell cycle. The neck localization is mediated mainly by an interaction between the second coiled-coil region in the N-terminus and the septin Cdc10, whereas the localization to the sites of polarized growth is mediated entirely by the F-BAR domain. In contrast, the C-terminal half of Hof1 interacts with Myo1, the sole myosin-II heavy chain in budding yeast, and localizes to the bud neck in a Myo1-dependent manner from the onset to the completion of cytokinesis. We also show that the SH3 domain in the C-terminus plays an important role in maintaining the symmetry of Myo1 ring constriction during cytokinesis and that Hof1 interacts with Chs2, a chitin synthase that is required for primary septum formation. Together these data define a mechanism that accounts for the localization of Hof1 during the cell cycle and suggest that Hof1 may function in cytokinesis by coupling actomyosin ring constriction to primary septum formation through interactions with Myo1 and Chs2.**

Monitoring Editor
Fred Chang
Columbia University

Received: Nov 13, 2012
Revised: Feb 15, 2013
Accepted: Feb 22, 2013

INTRODUCTION

Cytokinesis in animal and fungal cells requires the function and spatiotemporal coordination of a cortical actomyosin ring (AMR) and targeted membrane deposition (Balasubramanian *et al.*, 2004; Barr and Gruneberg, 2007; Pollard, 2010). The AMR is believed to generate a contractile force that powers the ingression of the plasma membrane (PM). At the same time, targeted exocytosis is believed to increase cell-surface area and deliver enzymatic cargoes for localized extracellular matrix (ECM) remodeling during cytokinesis. Although numerous components have been implicated in cytokinesis, the molecular mechanisms underlying their specific functions are largely unknown.

In the budding yeast *Saccharomyces cerevisiae*, efficient cytokinesis requires the coordinated actions of the AMR and septum formation (Wloka and Bi, 2012). The AMR consists of actin filaments and the sole myosin-II heavy chain Myo1. Although cells lacking Myo1 are viable in most strain backgrounds, they do display extensive defects in cytokinesis and cell separation (Watts *et al.*, 1987; Rodriguez and Paterson, 1990; Bi *et al.*, 1998; Lippincott and Li, 1998a). AMR constriction is followed by the centripetal growth of a primary septum (PS) that is catalyzed by the chitin synthase II Chs2. Chs2 is a transmembrane cargo whose expression, localization,

This article was published online ahead of print in MBoC in Press (http://www.molbiolcell.org/cgi/doi/10.1091/mbc.E12-11-0804) on March 6, 2013.

*Present address: Graduate School of Biostudies, Kyoto University, Kyoto 606-8502, Japan.

Address correspondence to: Erfei Bi (ebi@mail.med.upenn.edu).

Abbreviations used: AMR, actomyosin ring; PM, plasma membrane; PS, primary septum.

and activation at the division site are elaborately regulated by exocytic machinery (Chuang and Schekman, 1996; VerPlank and Li, 2005) and cell cycle kinases and phosphatases, including CDK1 and the kinases (Cdc5, Cdc15, Dbf2, and Dbf20) and phosphatase (Cdc14) of the mitotic exit network (MEN; Zhang *et al.*, 2006; Teh *et al.*, 2009; Chin *et al.*, 2011; Oh *et al.*, 2012). Defects in PS formation cause asymmetric AMR constriction and severe defects in cytokinesis (Bi, 2001; Schmidt *et al.*, 2002; VerPlank and Li, 2005; Nishihama *et al.*, 2009). Several proteins, including Mlc1 (the essential light chain for Myo1 [Luo *et al.*, 2004] and also a light chain for myosin-Vs [Myo2 and Myo4 in budding yeast; Stevens and Davis, 1998] and IQGAP [Iqg1; Boyne *et al.*, 2000; Shannon and Li, 2000]), Iqg1 (Epp and Chant, 1997; Lippincott and Li, 1998a), Inn1 (a C2 domain- and PXXP motif-containing protein; Sanchez-Diaz *et al.*, 2008; Nishihama *et al.*, 2009; Meitinger *et al.*, 2010), Cyk3 (a transglutaminase-like protein; Korinek *et al.*, 2000; Nishihama *et al.*, 2009; Meitinger *et al.*, 2010), and Hof1 (an F-BAR protein that is the focus of this study; Kamei *et al.*, 1998; Lippincott and Li, 1998b; Vallen *et al.*, 2000; Meitinger *et al.*, 2010) have been implicated in AMR–PS coordination during cytokinesis, but the underlying mechanisms are poorly understood.

Septins are filament-forming, GTP-binding proteins that are conserved from yeast to humans (Weirich *et al.*, 2008; McMurray and Thorner, 2009; Oh and Bi, 2011). The five mitotic septins in budding yeast (Cdc3, Cdc10, Cdc11, Cdc12, and Shs1) form two octameric complexes (Cdc11-Cdc12-Cdc3-Cdc10-Cdc10-Cdc3-Cdc12-Cdc11 and Shs1-Cdc12-Cdc3-Cdc10-Cdc10-Cdc3-Cdc12-Shs1) that promote linear filament and ring assembly in vitro, respectively (Garcia *et al.*, 2011). Septin filaments are organized into an hourglass structure at the bud neck before cytokinesis. This structure is triggered by the MEN to split into two cortical rings that sandwich the AMR during cytokinesis (Lippincott *et al.*, 2001). Septins play at last two distinct roles in cytokinesis in budding yeast. Before the onset of cytokinesis, the septin hourglass acts as a scaffold required for AMR assembly (Bi *et al.*, 1998; Lippincott and Li, 1998a). During cytokinesis, the septin double ring is believed to act as a diffusion barrier (Dobbelaere and Barral, 2004) and shares an essential role with the AMR in restricting cytokinesis factors to the division site (Wloka *et al.*, 2011). Thus septins are required for AMR function, as well as for PS formation. Nearly all bud neck–localized proteins depend on septins for their localization (Gladfelter *et al.*, 2001), but in most cases how septins interact with these associated proteins is not well understood.

Like most F-BAR proteins, Hof1 contains an F-BAR domain at its N-terminus and an SH3 domain at its C terminus (Heath and Insall, 2008; Suetsugu *et al.*, 2010). F-BAR proteins are generally involved in clathrin-mediated endocytosis by coupling the PM to the actin cytoskeleton (Itoh *et al.*, 2005; Tsujita *et al.*, 2006; Shimada *et al.*, 2007). The F-BAR domain forms a banana-shaped dimer that tubulates the PM by interacting with phospholipids such as phosphatidylserine and phosphatidylinositol 4,5-bisphosphate, whereas the SH3 domain interacts with N-WASP and dynamin, which promote Arp2/3-nucleated actin polymerization and membrane scission during endocytosis. Unlike these F-BAR proteins, Hof1 functions in cytokinesis. It localizes to the division site in a complex pattern during the cell cycle (Lippincott and Li, 1998b; Vallen *et al.*, 2000). Specifically, Hof1 localizes to the bud neck, preferentially at the mother side, from S/G2 to anaphase in a septin-dependent manner. Around the onset of cytokinesis, Hof1 briefly localizes to both sides of the bud neck with nearly equal intensity and then associates with the AMR between the septin rings during cytokinesis. The switch in Hof1 localization from septin-based structures to the AMR appears to be correlated with its peak phosphorylation during the cell cycle (Vallen *et al.*, 2000), which is catalyzed by several kinases, including CDK1 (Cdc28), Cdc5 (Polo kinase), and Dbf2/Dbf20-Mob1 (Meitinger *et al.*, 2011). After cytokinesis, a fraction of Hof1 lingers at the division site momentarily before its full disappearance. The reduction of Hof1 at the division site during and after cytokinesis is carried out by ubiquitin-mediated proteasomal degradation in G1, which depends on the PEST sequence of Hof1 (Blondel *et al.*, 2005). Deletion of *HOF1* causes temperature-sensitive growth, with cells arrested in cytokinesis at the nonpermissive temperature (Kamei *et al.*, 1998; Lippincott and Li, 1998b; Vallen *et al.*, 2000). In addition, deletion of *HOF1* does not appear to affect AMR assembly (Vallen *et al.*, 2000) but does cause asymmetric PS formation (Meitinger *et al.*, 2011). Furthermore, *hof1Δ* and *myo1Δ* are synthetically lethal (Vallen *et al.*, 2000). Taken together, these observations suggest that Hof1 may function in cytokinesis by coupling the AMR to PS formation. Despite the progress made in understanding Hof1, the molecular mechanisms underlying its complex localization pattern during the cell cycle and its potential involvement in the AMR-PS coupling during cytokinesis are unknown.

In this study, we show that Hof1 contains three distinct targeting domains that are differentially required for cytokinesis. Hof1 targets to the division site before cytokinesis by interacting with septins and during cytokinesis by interacting with Myo1. In addition, Hof1 is involved in the AMR–PS coordination during cytokinesis, at least in part, by interacting with both Myo1 and Chs2 directly.

RESULTS

The N- and C-terminal halves of Hof1 play distinct roles in cytokinesis

To determine how Hof1 is involved in cytokinesis, we performed a structure–function analysis. Hof1 was divided into halves: the N-terminal half (Hof1-N-term; 1–340), containing the conserved *pombe* Cdc15 homology (PCH) sequence and coiled-coil (CC1 and CC2) regions, and the C-terminal half (Hof1-C-term; 341–669), containing the PEST sequence and Src homology 3 (SH3) domain (Figure 1A). Because the PEST sequence is known to mediate Hof1 degradation during and after cytokinesis (Blondel *et al.*, 2005) and the SH3 domain interacts with Inn1, a protein required for PS formation during cytokinesis (Nishihama *et al.*, 2009), we also generated *hof1* alleles lacking the coding sequences for these protein motifs (Hof1-PESTΔ; Hof1-SH3Δ) to assess their roles in cytokinesis.

Centromere-based, *LEU2*-marked plasmids carrying different *HOF1* alleles (see foregoing) under the control of the *HOF1* promoter were introduced into a host strain containing *hof1Δ*, *cyk3Δ*, and a *URA3*-marked cover plasmid carrying wild-type *HOF1*. *CYK3* encodes a protein that shares an essential role with Hof1 in cytokinesis, as *hof1Δ* and *cyk3Δ* are synthetically lethal with cells arrested in cytokinesis (Korinek *et al.*, 2000). Thus any *HOF1* allele that enables the host strain to form colonies on plates containing 5-fluoroorotic acid (5-FOA), which selects against the presence of the cover plasmid (or Ura^+ cells), would be deemed functional in cytokinesis (Figure 1B). As expected, the plasmid carrying the full-length *HOF1*, but not the empty vector, complemented the *hof1Δ cyk3Δ* mutant. Hof1 lacking either the PEST sequence or the SH3 domain also complemented the double mutant, suggesting that these sequence motifs are not essential for Hof1 function. However, these results do not rule out the possibility that the PEST sequence and the SH3 domain may play some nonessential but nevertheless important regulatory roles. Of interest, Hof1-C-term consistently complemented the double mutant, albeit to a much lesser degree than full-length *HOF1*; in contrast, Hof1-N-term completely failed to

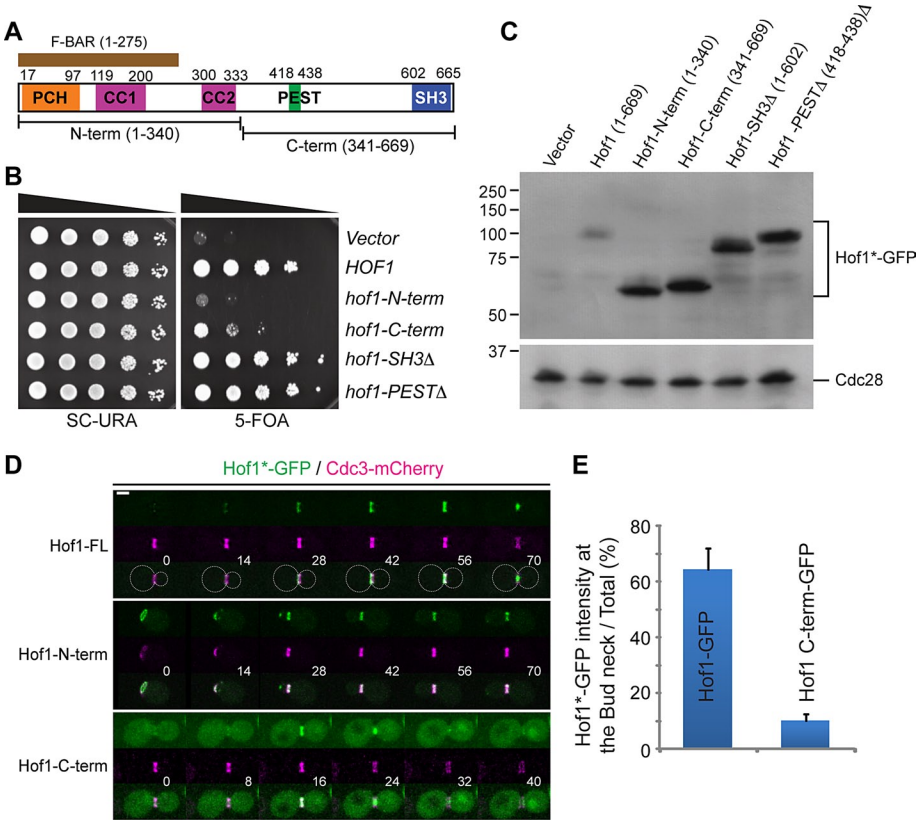

FIGURE 1: Hof1-N-term and Hof1-C-term display distinct localization patterns during the cell cycle and are differentially required for cytokinesis. (A) Schematic diagram of Hof1 in budding yeast. All major domains, motifs, and conserved sequences are indicated. (B) Differential roles of different Hof1 domains or motifs in cytokinesis. Tenfold serial dilutions of the *hof1Δ cyk3Δ* [pRS316-HOF1] strains (YEF4970, YEF4966, YEF4945, YEF4949, YEF4944, and YEF 4948) carrying plasmids harboring different truncated alleles of *HOF1* expressed from the *HOF1* promoter were spotted onto either SC-URA or 5-FOA plate and incubated for 5 d at 25°C. (C) Comparable expression levels for different Hof1 fragments. The *hof1Δ* strains (YEF4909, YEF4551, YEF4554, YEF4913, YEF4552, and YEF4911) carrying plasmids expressing different GFP-Hof1 fragments from the *HOF1* promoter were grown to exponential phase in SC-LEU at 25°C, and the corresponding cell lysates were analyzed by Western blots using an anti-GFP (top) or an anti-Cdc28 antibody (bottom, as a loading control). Note that the full-length Hof1 was difficult to extract from an insoluble fraction. (D) Distinct localization patterns conferred by Hof1-N-term and Hof1-C-term. Cells of the *hof1Δ CDC3-mCherry* strains (YEF5479, YEF5421, and YEF5423) carrying centromere-based plasmids expressing different Hof1 fragments (Hof1-GFP, Hof1-N-term-GFP, and Hof1-C-term-GFP) from the *HOF1* promoter were grown to exponential phase in SC-LEU media at 25°C and then analyzed with time-lapse microscopy. Scale bar, 2 μm. (E) Targeting efficiencies of Hof1-C-term vs. the full-length protein. The signal ratios of Hof1-GFP ($n = 11$) and Hof1-C-term-GFP ($n = 11$) at the bud neck vs. the whole cell before the septin-hourglass splitting were quantified. Error bars, SDs.

complement, even though both alleles were expressed at comparable levels (Figure 1C). These data suggest that the C-terminal half of Hof1 is more critical for cytokinesis, whereas the N-terminal half makes an important yet undefined contribution to the same process.

To explore how Hof1-N-term and Hof1-C-term contribute to cytokinesis differently, we determined their localization by time-lapse microscopy. As reported previously (Lippincott and Li, 1998b; Vallen *et al.*, 2000), full-length Hof1–green fluorescent protein (GFP) began its localization at the mother side of the bud neck during S/G2 phase, became equalized in intensity at both sides of the bud neck shortly before cytokinesis, and finally associated with the AMR during cytokinesis (Figure 1D, top, and Supplemental Video S1, top). In contrast, Hof1-N-term–GFP and Hof1-C-term–GFP, expressed from the *HOF1* promoter in *hof1Δ* cells, displayed distinct patterns of localization during the cell cycle. Hof1-N-term–GFP always associated with septin structures at the bud neck throughout the cell cycle (Figure 1D, middle, and Supplemental Video S1, middle; also see later discussion of Figure 4D, left). Its apparent colocalization with the old septin ring in G1 cells is presumably caused by the lack of PEST sequence–mediated degradation (Figure 1D, middle, 0 min; the old septin ring is always larger in diameter than the subsequently assembled new septin ring at the presumptive bud site; Blondel *et al.*, 2005). A fraction of Hof1-N-term–GFP also localized to the bud cortex during the early stage of budding. In addition, Hof1-N-term–GFP localized as a broad band between the septin rings during cytokinesis (see Figure 4D, left, cell 4). These data suggest that Hof1-N-term has the capacity to interact with septins or septin-associated proteins, as well as with some factors associated with the bud cortex or the bud neck.

Strikingly, Hof1-C-term–GFP localized to the bud neck shortly before the splitting of the septin hourglass into two cortical rings (Figure 1D, bottom, and Supplemental Video S1, bottom)—a cellular event that marks the onset of mitotic exit and cytokinesis (Lippincott *et al.*, 2001)—and then constricted like the full-length protein. Immediately after cytokinesis, Hof1-C-term–GFP disappeared from the bud neck. This localization profile is consistent with its functional requirement in cytokinesis (Figure 1B). Of importance, 64% of the total Hof1-GFP signal was localized at the bud neck 2–4 min before cytokinesis; in contrast, only 10% of the total Hof1-C-term–GFP was observed at the bud neck at the same cell cycle stage (Figure 1E). This result suggests that the N-terminus of Hof1 can greatly facilitate the accumulation of Hof1 at the bud neck. Taken together, these data indicate that the two halves of Hof1 play distinct roles in cytokinesis.

The N-terminus of Hof1 localizes to the bud neck and binds to septin complexes in a Cdc10-dependent manner

The localization profile of Hof1-N-term during the cell cycle suggests an interaction with septins. To test this possibility, we performed in vitro binding assays using recombinant proteins purified from *Escherichia coli* (Figure 2, A and B). The full-length Hof1 fused to the bacterial maltose-binding protein (MBP–Hof1-FL) and MBP–Hof1-N-term bound strongly to the five-septin complex (Cdc3, Cdc10, Cdc11, hexahistidine [His_6]-Cdc12, and Shs1) in buffers containing100 mM NaCl but not 300 mM NaCl. Under the same condition, MBP–Hof1-C-term showed a very weak interaction, whereas MBP and MBP-Cyk3 (controls) failed to interact with the septin complexes completely. Because septin complexes are known to form filaments under the low-salt, but not the high-salt, condition

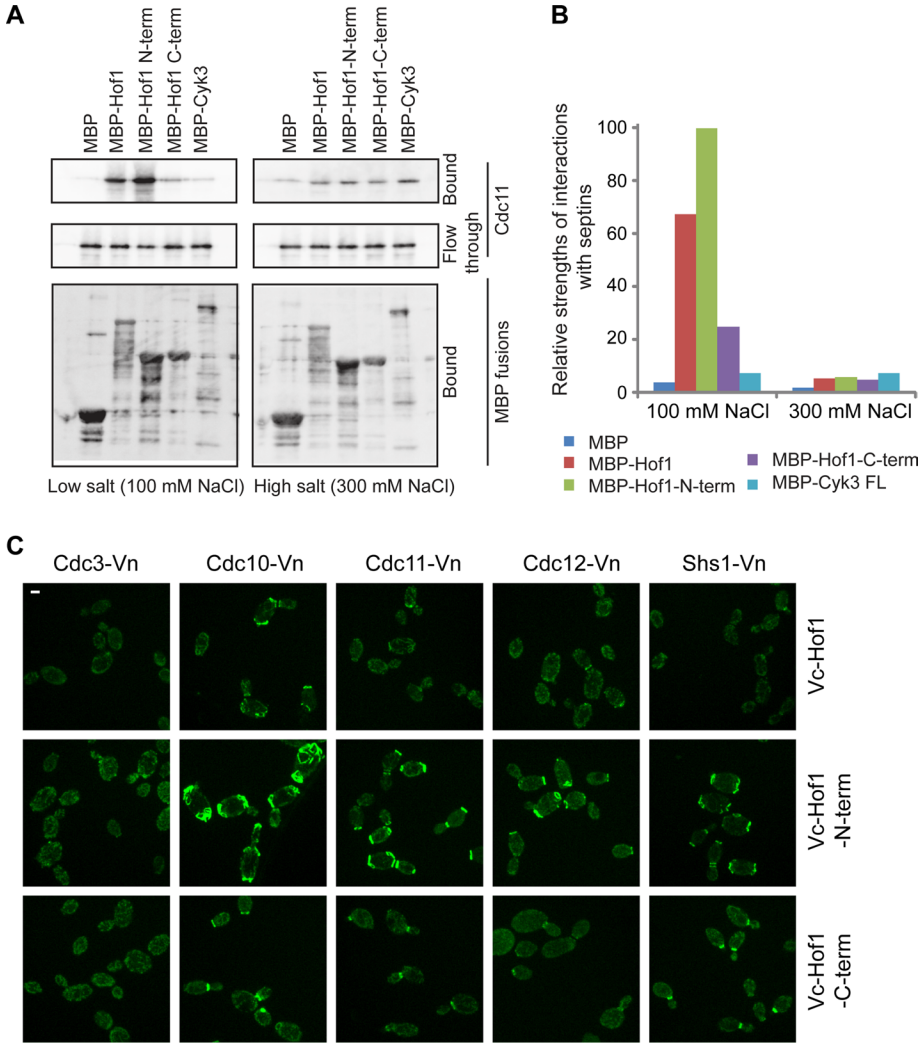

FIGURE 2: Hof1-N-term binds to septin complexes in vitro and in vivo. (A) Hof1-N-term binds to septin complexes in vitro. Recombinant MBP-Hof1* fusion proteins (MBP-Hof1, MBP-Hof1-N-term, and MBP-Hof1-C-term), along with the controls (MBP and MBP-Cyk3), were used in the in vitro binding assays to assess their interactions with the five-septin complexes (Cdc3, Cdc10, Cdc11, His_6-Cdc12, and Shs1) under salt conditions that either favor (100 mM NaCl) or prevent (300 mM NaCl) filament assembly. (B) Relative strengths of interactions between Hof1 fragments and septin complexes. The binding data from A were used for quantitative analysis. (C) Hof1-N-term binds to septins in vivo. The BiFC assay was used to determine the interactions between different Hof1 fragments and septin subunits in vivo. MATa strains each containing a specific septin gene C-terminally tagged with the N-terminus of Venus (septin-Vn) were mated pairwise with MATα strains each containing a specific *hof1* fragment N-terminally tagged with the C terminus of Venus (Vc-Hof1*). The resulting diploid strains were monitored for yellow fluorescence signals, which reflect the relative strengths of interactions between Hof1 fragments and septin subunits. For interactions between Hof1 and septins, strains YEF5812, YEF5813, YEF5814, YEF5815, and YEF5816 were used; for interactions between Hof1-N-term and septins, YEF5883, YEF5881, YEF5884, YEF5885, and YEF5886 were used; for interactions between Hof1-C-term and septins, YEF5930, YEF5934, YEF5931, YEF5932, and YEF5933 were used. Scale bar, 2 μm.

(Frazier *et al.*, 1998; Versele *et al.*, 2004), these data suggest that Hof1-N-term may bind preferentially to septin filaments in vitro. Alternatively, the interaction between Hof1-N-term and the septin complexes is of relatively low affinity and therefore is salt sensitive. We also found that the binding of MBP-Hof1-FL and MBP-Hof1-N-term to septin complexes is independent of Shs1 (unpublished data), the septin subunit known to promote septin ring and gauze formation in vitro (Garcia *et al.*, 2011).

To determine whether Hof1-N-term interacts with septins in vivo, we performed a bimolecular fluorescence complementation (BiFC) assay (Kerppola, 2008). Different yeast haploid strains each containing a specific septin subunit C-terminally tagged with the N-terminus of Venus (yellow fluorescence protein; septin-Vn) were crossed with yeast strains of the opposite mating type each containing a specific Hof1 fragment (full-length, Hof1-N-term, and Hof1-C-term) N-terminally tagged with the C terminus of Venus (Vc-Hof1*) to generate diploid strains. Fluorescence signals were monitored in the diploids to determine the interactions between different Hof1 fragments and septin subunits. Consistent with the in vitro binding data, Hof1-N-term clearly displayed stronger interactions with various septin subunits than either full-length Hof1 or Hof1-C-term (Figure 2C). In addition, Cdc10 consistently generated the strongest BiFC signals with different Hof1 fragments, particularly with Hof1-N-term. On the contrary, Cdc3 failed to interact with any of the Hof1 fragments in this assay. Strikingly, Hof1-N-term appeared to interact with cable-like "septin filaments" (Figure 2C; Cdc10-Vn × Vc-Hof1-N-term), which are presumably formed due to compromised Cdc10 functionality by tagging, as well as the "locking" effect of BiFC (Kerppola, 2008). Despite the caveats associated with this assay, the BiFC data clearly indicate that Hof1-N-term is capable of interacting with the septins in vivo, in particular, the Cdc10 subunit.

If Hof1-N-term interacts with septin complexes and/or filaments mainly through Cdc10, Hof1-N-term may not be able to localize to the bud neck in cells deleted for *CDC10*. Indeed, Hof1-N-term–GFP failed to localize to the bud neck in all *cdc10Δ* cells before the onset of cytokinesis, despite the localization of the rest of the septins to the division site (Figure 3A and Supplemental Video S2) and their ability to form complexes and filaments (McMurray *et al.*, 2011). During cytokinesis, Hof1-N-term–GFP localized to the bud neck (unpublished data), presumably by dimerizing with the endogenous Hof1 that is associated with the AMR, as the F-BAR domain (1–275) in Hof1-N-term (Figure 1A) is known to form dimers in vitro (Moravcevic, Alvarado, Schmitz, Kenniston, Mendrola, and Lemmon, personal communication). In sharp contrast, Hof1-N-term–GFP localized to the bud neck in *cdc11Δ* and *shs1Δ* cells before the onset of cytokinesis, even though the *cdc11Δ* cells display poorer viability and more severe defects in cytokinesis than the *cdc10Δ* cells (Frazier *et al.*, 1998). These data suggest that Hof1-N-term may localize to the bud neck by interacting with Cdc10. To test this possibility, we performed in vitro binding assays. Indeed, in comparison to the four-septin complex (Cdc3, Cdc10, Cdc11, and His_6-Cdc12), the

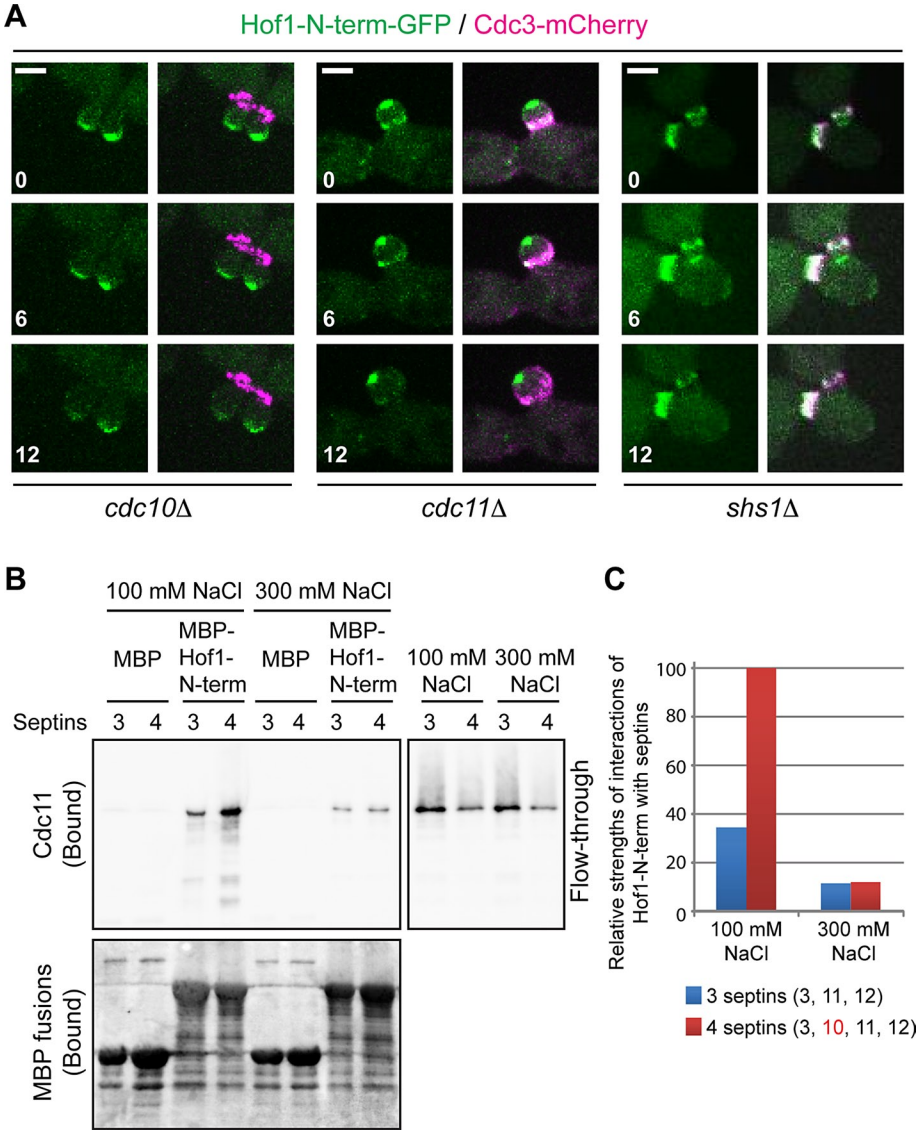

FIGURE 3: Hof1-N-term localizes to the bud neck and binds to septin complexes in a Cdc10-dependent manner. (A) Hof1-N-term fails to localize to the bud neck before the onset of cytokinesis in *cdc10Δ* cells. Viable septin deletion strains (YEF6532, *cdc10Δ*; YO1542, *cdc11Δ*; and YO1538, *shs1Δ*) containing *CDC3-mCherry* and expressing Hof1-N-term–GFP from its own promoter were grown in SC-LEU media at 25°C and then imaged by time-lapse microscopy. Selected frames from representative time-lapse series were chosen to show the neck localization of Hof1-N-term in different septin mutants before cytokinesis. Scale bar, 2 μm. (B) The interaction between Hof1-N-term and septin complexes is significantly reduced in the absence of Cdc10. The in vitro binding assays were performed as described in Figure 2A, except that only two MBP fusion proteins (MBP and MBP-Hof1-N-term) and two different septin complexes (the three-septin complex [Cdc3, Cdc11, and His_6-Cdc12] and the four-septin complex [Cdc3, Cdc10, Cdc11, and His_6-Cdc12]) were used. (C) Quantification of the binding data in B.

three-septin complex (Cdc3, Cdc11, and His_6-Cdc12) displayed a marked reduction in its interaction with Hof1-N-term (Figure 3, B and C). Taken together, these data indicate that Hof1-N-term localizes to the bud neck and interacts with the septin complexes and/or filaments in a Cdc10-dependent manner. Although it is likely that Hof1-N-term interacts directly with Cdc10 as suggested by previous two-hybrid analysis (Meitinger *et al.*, 2011), our data do not rule out the possibility that the requirement of Cdc10 in Hof1-N-term localization and its interaction with the septin complexes may simply reflect an essential role of Cdc10 in the robustness of septin filament assembly in vitro and in vivo (Frazier *et al.*, 1998; McMurray *et al.*, 2011).

The second coiled-coil region mediates the bud neck localization and septin binding of the Hof1 N-terminus

To further narrow down which region of Hof1-N-term is required for bud neck localization and septin binding, we divided this fragment into the F-BAR domain (1–275), whose boundary has been determined experimentally (Moravcevic *et al.*, personal communication), and a smaller fragment (276–340) containing the CC2 region (referred to as Hof1-CC2 hereafter; Figure 1A). Our in vitro binding assay showed that the Hof1-CC2 fragment retained significant ability to bind septin complexes, whereas the F-BAR domain displayed a weak interaction that was slightly greater than that for the MBP control (Figure 4, A and B). The interaction between Hof1-CC2 and the septins was also found independently by another group (Meitinger *et al.*, 2013). Consistent with these binding data, we found that overexpression of Hof1-N-term disrupted septin structures at the bud neck, whereas overexpression of the F-BAR domain did not (Figure 4C). In addition, we found that Hof1-CC2–GFP colocalized with the septins at the bud neck in *hof1Δ* cells throughout the cell cycle (Figure 4D). However, in comparison to Hof1-N-term–GFP, the ratio of neck-localized signal versus total signal for Hof1-CC2-GFP was significantly reduced (~4.5-fold; Figure 4E), which is also consistent with the binding data (Figure 4, A and B). Of interest, Hof1–F-BAR–GFP did not localize to the bud neck from G1 to telophase (Figure 4F), despite its comparable level of expression to Hof1-CC2 and Hof1-N-term (Figure 4I). Instead, Hof1–F-BAR–GFP localized to the bud cortex upon bud emergence and disappeared gradually from the cortex before cytokinesis (Figure 4F). During cytokinesis, Hof1–F-BAR–GFP localized as a broad band between the septin rings and did not appear to display an AMR-like constriction (Figure 4, F and G, cell 4, and H). In postcytokinesis cells (after the completion of AMR constriction), Hof1–F-BAR–GFP localized within the old septin rings as a disk (Figure 4G, cell 5, the large disk) and also as a disk within the nascent septin ring at the presumptive bud site (Figure 4G, cell 5, the small disk). Taken together, these data indicate that the F-BAR domain and the CC2 region mediate the cortical and bud neck localizations of Hof1-N-term, respectively, with the CC2 region being chiefly responsible for the interaction of Hof1-N-term with septin complexes.

To determine the role of CC2-mediated septin binding in cytokinesis, we generated a Hof1 mutant lacking the CC2-coding region (Hof1-CC2Δ) and then assessed its functionality and localization profile throughout the cell cycle. Surprisingly, Hof1-CC2Δ complemented both the *hof1Δ cyk3Δ* and *hof1Δ myo1Δ* double mutants efficiently (Supplemental Figure S1, A and B), suggesting that the

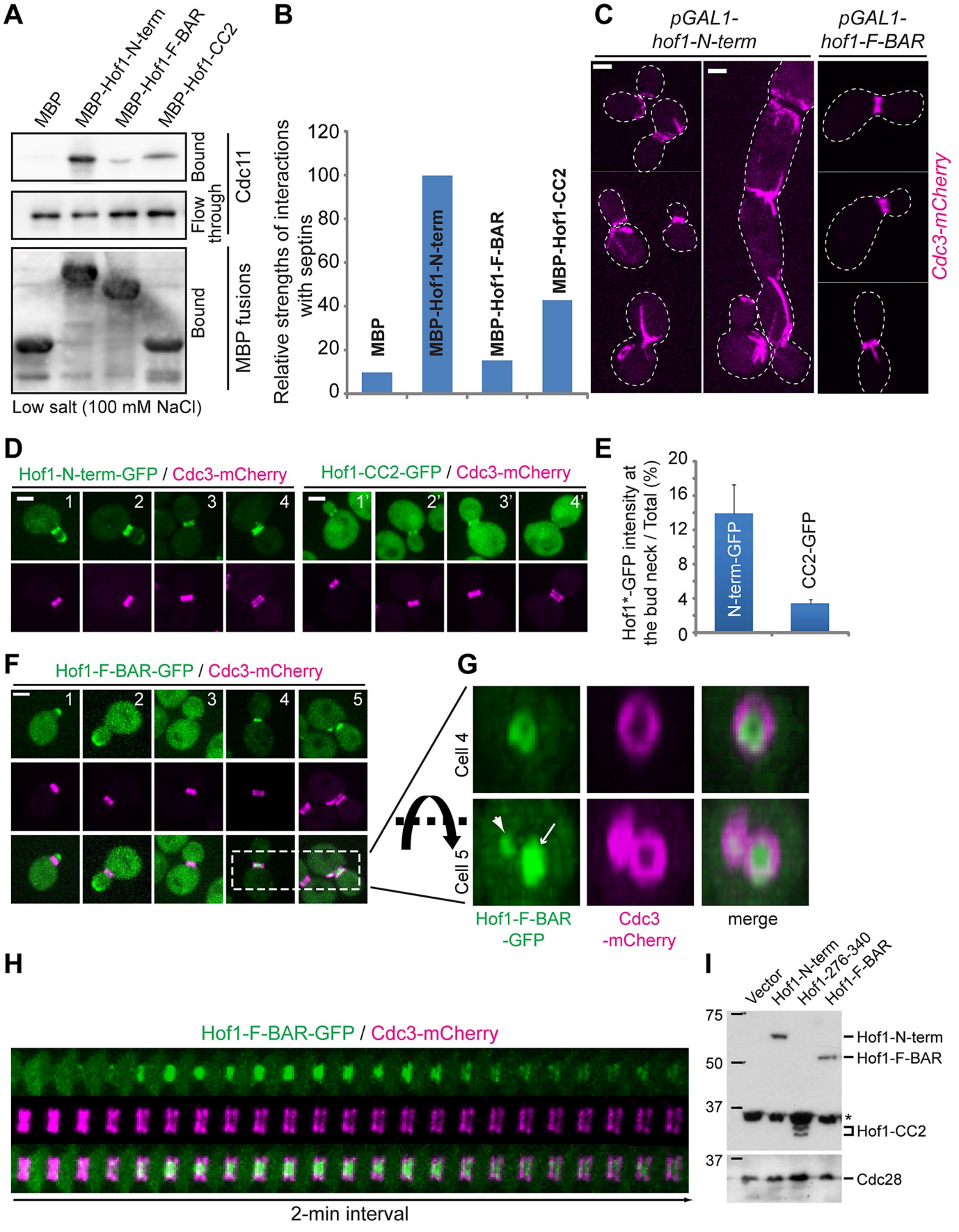
A
MBP
MBP-Hof1-N-term
MBP-Hof1-F-BAR
MBP-Hof1-CC2
Bound
Flow through
Cdc11
Bound
MBP fusions
Low salt (100 mM NaCl)
B
Relative strengths of interactions with septins
120
100
80
60
40
20
0
MBP
MBP-Hof1-N-term
MBP-Hof1-F-BAR
MBP-Hof1-CC2
C
pGAL1-hof1-N-term
pGAL1-hof1-F-BAR
Cdc3-mCherry
D
Hof1-N-term-GFP / Cdc3-mCherry
Hof1-CC2-GFP / Cdc3-mCherry
1
2
3
4
1'
2'
3'
4'
E
Hof1*-GFP intensity at the bud neck / Total (%)
20
16
12
8
4
0
N-term-GFP
CC2-GFP
F
Hof1-F-BAR-GFP / Cdc3-mCherry
1
2
3
4
5
G
Cell 4
Cell 5
Hof1-F-BAR -GFP
Cdc3 -mCherry
merge
H
Hof1-F-BAR-GFP / Cdc3-mCherry
2-min interval
I
Vector
Hof1-N-term
Hof1-276-340
Hof1-F-BAR
75
50
37
37
Hof1-N-term
Hof1-F-BAR
*
Hof1-CC2
Cdc28

CC2 region is dispensable for cytokinesis. Hof1-CC2Δ–GFP localized to the bud neck earlier than Hof1-C-term–GFP during the cell cycle (~14 and 8 min before septin-hourglass splitting, respectively; Supplemental Figure S1C and Supplemental Video S3). Of importance, a higher fraction of Hof1-CC2Δ–GFP (36.8 ± 6.8%, n = 10) accumulated at the bud neck 2–4 min before cytokinesis than did Hof1-C-term–GFP (9.9 ± 2.5%, n = 11; Figure 1E), which may explain why Hof1-CC2Δ can carry out cytokinesis function more effectively than Hof1-C-term. Alternatively, the F-BAR domain in Hof1-CC2Δ may contribute to cytokinesis by an undefined mechanism.

The C-terminus of Hof1 interacts with Myo1 during cytokinesis

As shown earlier (Figure 1D, bottom), Hof1-C-term localized to the bud neck just before cytokinesis and constricted during cytokinesis, suggesting that Hof1-C-term may associate with AMR components. To test this possibility, we examined the localization of Hof1-C-term in *myo1Δ* cells, as Myo1 plays an essential role in AMR assembly (Bi *et al.*, 1998; Lippincott and Li, 1998a). As expected, Hof1-C-term failed to localize and constrict at the center position between the septin rings during cytokinesis (Figure 5A and Supplemental Video S4). Instead, it was associated with the septin rings themselves, with a preferential enrichment at either the mother or the daughter side. This localization pattern is consistent with the weak interactions observed between Hof1-C-term and septin complexes in vitro (Figure 2, A and B) and in vivo (Figure 2C). Of importance, as long as Myo1 was present, Hof1-C-term preferentially associated with the AMR even when the latter constricted asymmetrically in *cdc10Δ* or *chs2Δ* cells (Figure 5A and Supplemental Video S4; VerPlank and Li, 2005; Wloka *et al.*, 2011). Like Myo1 (Bi *et al.*, 1998; Tully *et al.*, 2009), we also found that Hof1-C-term localized to the division site in an F-actin–independent manner, as indicated by its localization and gradual disappearance from the division site without constriction in cells treated with latrunculin A (Ayscough *et al.*, 1997; Figure 5B and Supplemental Video S5). These data suggest that Hof1-C-term may interact with Myo1 or Myo1-associated proteins. Indeed, our in vitro binding experiment showed that Hof1-C-term was able to interact with Myo1-tail (856–1928; Figure 5C), which harbors all the targeting domains (TD1 and TD2) for the localization of Myo1 to the division site (Fang *et al.*, 2010). This interaction was relatively weak in comparison to the positive control Bni5, which is known to display a robust interaction with Myo1-tail or Myo1-TD1 (856–1223, 1398–1928) but not with Myo1-TD2 (1224–1397; Figure 5C; Fang *et al.*, 2010). Thus Hof1-C-term associates with the AMR during cytokinesis, at least in part, by interacting with Myo1-tail.

The SH3 domain of Hof1 is important for maintaining the symmetry of Myo1 ring constriction

Overexpression of the full-length Hof1 is known to cause pronounced defects in cytokinesis and septin organization (Lippincott and Li, 1998b). However, it remains unknown whether the cytokinesis defect is secondary to the septin defect, as septins are essential for cytokinesis in budding yeast (Hartwell, 1971; Wloka and Bi, 2012). To gain further insight into how the N- and C-terminal halves of Hof1 play distinct roles in cytokinesis, we analyzed their overexpression effects. Consistent with our observations that Hof1-N-term interacts with septins throughout the cell cycle and Hof1-C-term interacts with Myo1 during cytokinesis, we found that overexpression of Hof1-N-term disrupted septin organization and caused cytokinesis defects (Figure 4C, left), whereas overexpression of Hof1-C-term caused cytokinesis defects without septin disruption (Figure 6, A and B; and unpublished data). Because the SH3 domain in Hof1-C-term binds to the PXXP motifs in Inn1 and Cyk3, two proteins involved in PS formation during cytokinesis (Nishihama *et al.*, 2009; Labedzka *et al.*, 2012), we also monitored the overexpression effect of Hof1-C-term lacking the SH3 domain (Hof1-C-term-SH3Δ) and found that the percentage of cells defective in cytokinesis (cell clusters with three or more connected cell bodies) was reduced from 90 to 50% (Figure 6, A and B), suggesting that both the SH3 domain and the rest of the C-terminus contribute to the cytokinesis defects. The importance of the SH3 domain in cytokinesis is further supported by the observation that Hof1 lacking the SH3 domain (Hof1-SH3Δ) failed to complement the synthetic lethality between *myo1Δ* and *hof1Δ* (Figure 6C; Vallen *et al.*, 2000).

FIGURE 4: The F-BAR domain and the second coiled-coil region of Hof1-N-term display distinct localization patterns and differential abilities in septin binding. (A) The CC2 region binds more strongly than the F-BAR domain to septin complexes. The indicated MBP fusion proteins were used in the in vitro binding assays as described in Figure 2A to assess their interactions with the five-septin complexes under low-salt condition. MBP-Hof1-N-term, MBP-Hof1–F-BAR, and MBP-Hof1-CC2 contain residues 1–340, 1–275, and 276–340 of Hof1, respectively. (B) Quantification of the binding data in A. (C) Overexpression of Hof1-N-term causes septin defects in an F-BAR–independent manner. Strains carrying *pGAL1* promoter-controlled Hof1-N-term (YO1834) or Hof1–F-BAR (YO1875) were grown in YM-1 rich media containing 2% galactose and 2% raffinose to induce the overexpression of the indicated Hof1 fragments at 25°C overnight and then documented for their cell morphologies and septin defects. Representative images are shown. (D) Hof1-CC2 localizes to the bud neck throughout the cell cycle. Strains carrying either Hof1-N-term–GFP or Hof1-CC2–GFP in *hof1Δ CDC3-mCherry* strains (YEF5421 and YO1878, respectively) were grown in SC-LEU media at 25°C and then imaged by fluorescence microscopy. (E) The targeting efficiency of Hof1-CC2 to the bud neck is much lower than that of Hof1-N-term. The signal ratios of Hof1-N-tern–GFP (n = 20) and Hof1-CC2-GFP (n = 20) at the bud neck vs. the total before the septin-hourglass splitting were quantified. (F) Hof1–F-BAR localizes to the sites of polarized growth during the cell cycle. Cells of a *hof1Δ CDC3-mCherry* strain (YO1880) expressing Hof1–F-BAR–GFP were grown in SC-LEU media at 25°C and then imaged by fluorescence microscopy. (G) Hof1–F-BAR associates with the PM between or within the septin rings during cytokinesis and cell polarization. Three-dimensional reconstructions of the cells 4 and 5 in F were performed and rotated along the indicated axis to show the association of the Hof1–F-BAR with the PM between or within the septin rings during early cytokinesis (cell 4, top), shortly after cytokinesis (cell 5, arrow), and at the presumptive bud site during cell polarization (cell 5, arrowhead). (H) Detailed analysis of Hof1–F-BAR association with the PM between the septin rings from telophase to the completion of cytokinesis. Time-lapse analysis was performed on strain YO1880 as described in Figure 1D. (I) Different Hof1 fragments are expressed at comparable levels. The expression levels of indicated GFP-Hof1* fragments in strains YEF4909, YEF5421, YO1878, and YO1879 were determined by Western blot analysis using anti-GFP and anti-Cdc28 (loading control) antibodies. Scale bars, 2 μm.

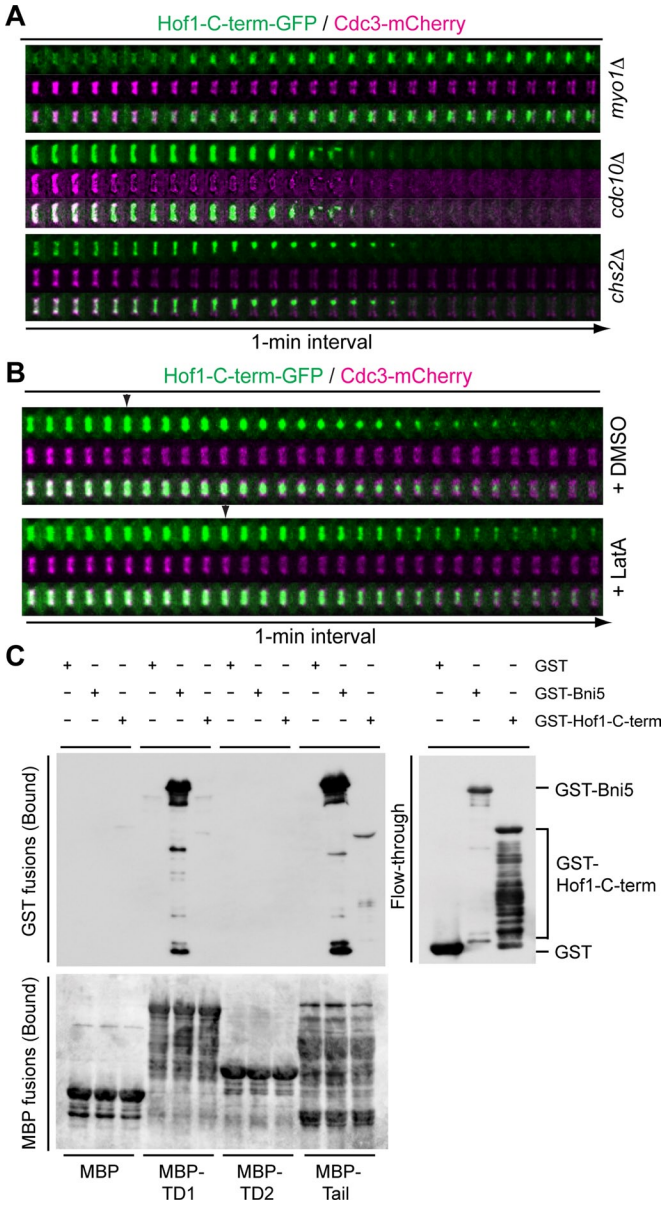

FIGURE 5: Hof1-C-term interacts with Myo1 tail in vitro and associates with Myo1 during cytokinesis. (A) The localization of Hof1-C-term to the midposition between the septin rings during cytokinesis requires Myo1 but not Cdc10 or Chs2. Hof1-C-term–GFP localization during cytokinesis was analyzed by time-lapse microscopy in various mutants carrying *CDC3-mCherry* (wild type [WT], YEF5422, data not shown due to its similarity to that in Figure 1D; *myo1Δ*, YEF6392; *cdc10Δ*, YO1473; *chs2Δ*, YEF6383). (B) Hof1-C-term localization to the division site is independent of F-actin. Cells of the strain YEF5422 were grown to exponential phase in SC-HIS media at 25°C, treated with either 200 μM LatA or DMSO for 30 min, and then followed by time-lapse microscopy. Arrowhead indicates septin-hourglass splitting. (C) Hof1-C-term binds to Myo1 tail in vitro. Recombinant GST–Hof1-C-term, together with the negative (GST) and positive (GST-Bni5) controls, was used in the in vitro binding assays to assess their interactions with different MBP-Myo1 tail fragments (MBP, negative control; MBP-Myo1-TD1; MBP-Myo1-TD2; and MBP-Myo1-tail).

We also found that overexpression of Hof1-C-term increased the duration of Myo1 ring constriction five times over the controls (wild-type and *hof1Δ* cells; Figure 6, D and E, and Supplementary Video S6). Strikingly, this increase was completely abolished by the deletion of the SH3 domain in the C-terminus (Figure 6, D and E, and Supplementary Video S6), suggesting that the SH3 domain is required for Myo1 stabilization at the division site during cytokinesis, which is consistent with the observed interaction between Hof1-C-term and Myo1-tail (Figure 5C). It is also possible that the SH3 domain may regulate Myo1 stability through PS formation, as overexpression of Hof1-C-term caused prolonged localization of Chs2 and Inn1 at the division site (unpublished data). Inn1 is a target of the SH3 domain required for PS formation (Nishihama *et al.*, 2009). Of interest, Myo1 ring displayed "asymmetric constriction" in ~50% of the *hof1Δ* cells carrying the *hof1-SH3Δ* allele ($n = 19$), which was expressed from its own promoter on a centromere-based plasmid (Figure 7, A and B). In contrast, Myo1 ring displayed "symmetric constriction" in 100% of the *hof1Δ* cells carrying the full-length *HOF1* ($n = 22$; Figure 7, A and B). Because the SH3 domain is known to interact with Inn1 and defects in PS formation such as those caused by deletion of *INN1* or *CHS2* often result in asymmetric Myo1 constriction (VerPlank and Li, 2005; Nishihama *et al.*, 2009; Oh *et al.*, 2012), it is likely that the asymmetric constriction observed in *hof1-SH3Δ* cells is due to elimination of the Hof1–Inn1 interaction or its resultant defect in PS formation. The duration of Myo1 ring constriction in the *hof1-SH3Δ* cells (11.3 ± 2.4 min, $n = 17$) was slightly longer than that in the *HOF1* control cells (9.5 ± 1.1 min, $n = 22$; Figure 7C). Taken together, these data suggest that the SH3 domain of Hof1 plays an important role in cytokinesis, at least in part by regulating the symmetry of Myo1 ring constriction.

Hof1 interacts with Chs2 and functions as a dosage suppressor of a *chs2* mutant

Hof1 is believed to function in cytokinesis by coupling AMR constriction to PS formation (Vallen *et al.*, 2000). In addition, deletion of *HOF1* clearly affects PS formation (Meitinger *et al.*, 2010). Thus we decided to explore the relationship between Hof1 and Chs2 during cytokinesis. Chs2 is phosphorylated at Ser-217 and Ser-225 at the division site by the Dbf2-Mob1 kinase during late stage of AMR constriction. This phosphorylation is believed to trigger Chs2 dissociation from the AMR in preparation for its eventual endocytic removal from the division site (Oh *et al.*, 2012). Surprisingly, high-copy *HOF1* suppressed the growth and cytokinesis defects of *chs2-DD* (phosphomimic form) but not *chs2-AA* (dephosphomimic form) cells (Figure 8A), suggesting that Hof1 may interact with Chs2 to promote its association with the AMR during cytokinesis. Indeed, the N-terminus of Chs2 (1–286) was able to interact with both Hof1-N-term and Hof1-C-term in vitro (Figure 8B). In addition, Chs2 became more mobile at the division site in *hof1Δ* cells, as analyzed by fluorescence recovery after photobleaching (FRAP), in contrast to wild-type cells, where Chs2 was immobile during AMR constriction (Figure 8, C and D, and Supplemental Video S7; Wloka *et al.*, 2013). Taken together with our observation that Hof1-C-term interacts with Myo1, these data suggest that Hof1 couples AMR constriction to PS formation during cytokinesis by interacting with both Myo1 and Chs2.

DISCUSSION

Hof1 contains multiple targeting domains that are differentially required for cytokinesis

In this study, we found that Hof1 contains multiple targeting domains that are differentially required for cytokinesis. Hof1-N-term localizes to the bud neck throughout the cell cycle. In addition, it localizes to the sites of polarized growth. However, Hof1-N-term by itself does not complement the cytokinesis defect of *hof1Δ cyk3Δ* cells. In contrast, Hof1-C-term localizes to the bud neck shortly before the onset

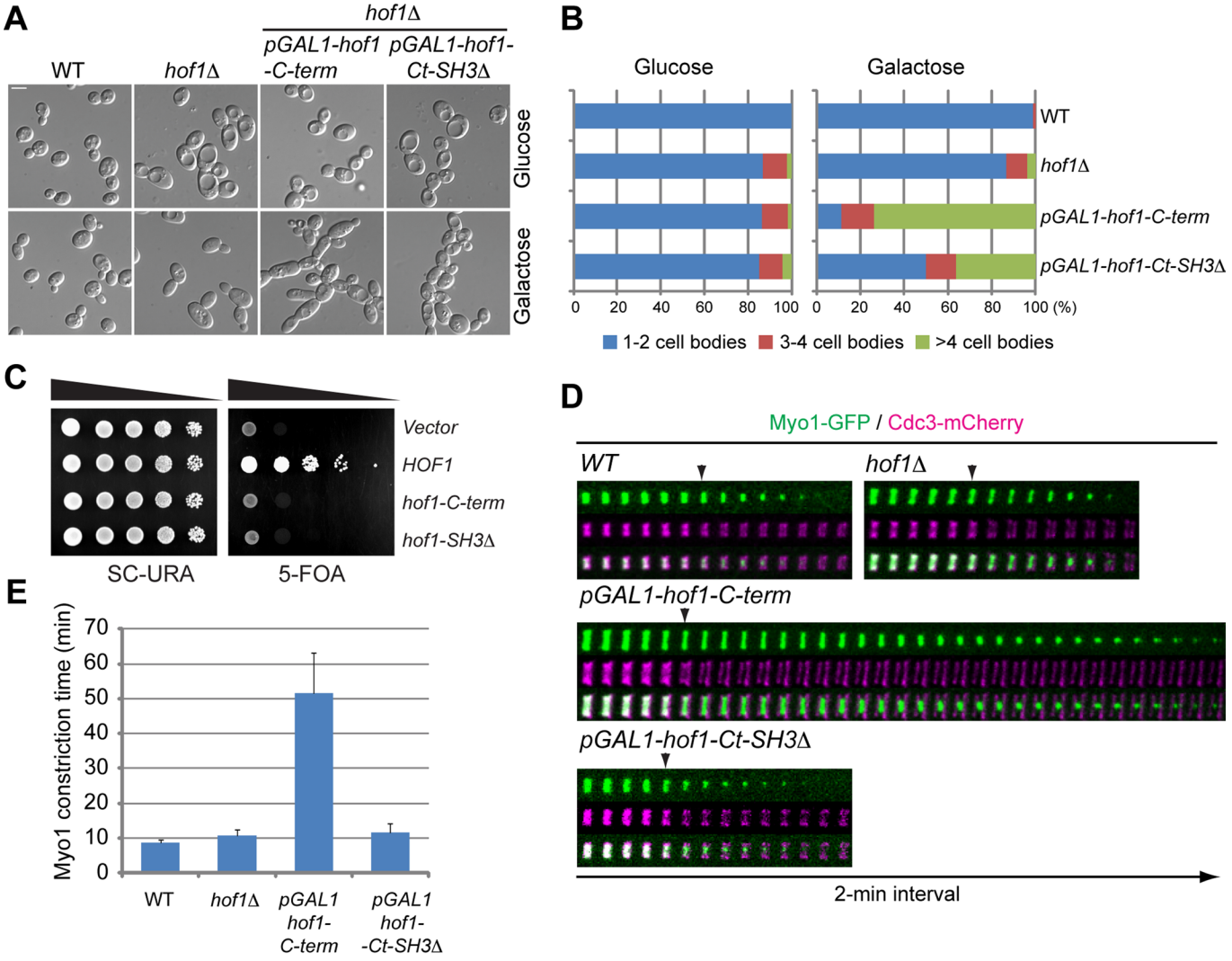

FIGURE 6: The SH3 domain plays an important role in cytokinesis and is required for Myo1 stabilization at the division site. (A) Overexpression of Hof1-C-term inhibits cytokinesis through the SH3 domain and the rest of the protein. Representative cell morphologies of different strains (WT, YO1860; *hof1Δ*, YO1864; *pGAL1-hof1-C-term*, YO1847; and *pGAL1-hof1-Ct-SH3Δ*, YO1870) carrying *MYO1-GFP* and *CDC3-mCherry* were imaged after growing in YM-1 rich media containing either 2% glucose (top) or 2% galactose and 2% raffinose (bottom) at 25°C overnight. Scale bar, 2 μm. (B) Quantification of cytokinesis defects displayed by the strains under the growth conditions specified in A. More than 200 cells were counted for each strain under each growth condition. (C) The SH3 domain of Hof1 is required for cytokinesis in the absence of *MYO1*. Tenfold-serial dilutions of the *hof1Δ myo1Δ* [YCp50-MYO1] (YEF5451)–derived strains (YO1947, YO1948, YO1949, and YO1950) carrying plasmids harboring different truncated alleles of *HOF1* expressed from the *HOF1* promoter were spotted onto either SC-URA or 5-FOA plate and incubated for 3 d at 25°C. (D) Overexpression of Hof1-C-term causes Myo1 stabilization at the division site in an SH3 domain–dependent manner. Yeast strains described in A were grown in YM-1 rich media containing 2% galactose and 2% raffinose at 25°C and then analyzed for Myo1 ring constriction during cytokinesis by time-lapse microscopy. Arrowhead indicates septin-hourglass splitting. (E) Quantification of the duration of Myo1 ring constriction (from septin-hourglass splitting to the disappearance of Myo1-GFP signal from the division site) during cytokinesis using the data acquired in D (WT, $n = 4$; *hof1Δ*, $n = 6$; *pGAL1-hof1-C-term*, $n = 8$; and *pGAL1-hof1-Ct-SH3Δ*, $n = 5$).

of cytokinesis and is able to complement the cytokinesis defect of *hof1Δ cyk3Δ* cells, although its localization and complementation efficiencies are much lower than those of full-length Hof1. Thus both the N- and C-terminal portions of Hof1 are required for efficient cytokinesis. However, Hof1-C-term appears to play a more prominent role in cytokinesis, whereas Hof1-N-term contributes, at least, by promoting efficient targeting of Hof1 to the division site.

Hof1-N-term localizes to the bud neck and interacts directly with septin complexes in a Cdc10-dependent manner. This interaction accounts for the bud neck localization of Hof1 before the onset of cytokinesis. Further analysis indicates that Hof1-N-term contains two distinct targeting signals—the F-BAR domain and the CC2 region. The F-BAR domain localizes to sites of polarized growth, but its physiological target is unknown. The F-BAR domain forms a banana-shaped dimer like other F-BAR domains and binds nonselectively to phospholipid membranes with relatively low affinity (Moravcevic *et al.*, personal communication). It is possible that the F-BAR domain assumes the polarized localization in the cell by binding to locally

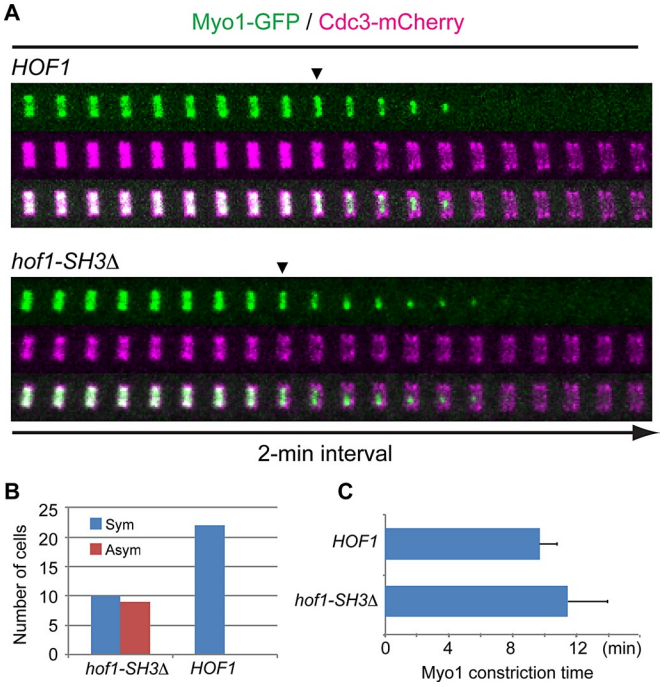

FIGURE 7: The SH3 domain plays an important role in maintaining the symmetry of Myo1 ring constriction. (A) Representative time-lapse series of Myo1-GFP constriction in the wild-type and *hof1-SH3Δ* cells. Cells of the *hof1Δ CDC3-mCherry* [pRS316-Myo1-C-GFP] strains (YO1966 and YO1967) carrying centromere-based plasmids expressing either *HOF1* (wild type) or *hof1-SH3Δ* from the *HOF1* promoter were grown to exponential phase in SC-LEU-URA media at 25°C and then analyzed by time-lapse microscopy. Arrowheads indicate the timing of septin-hourglass splitting. (B, C) Quantification of the symmetry (B) and duration (C; from septin-hourglass splitting to the disappearance of Myo1-GFP signal from the division site) of Myo1 ring constriction during cytokinesis using the data acquired in A.

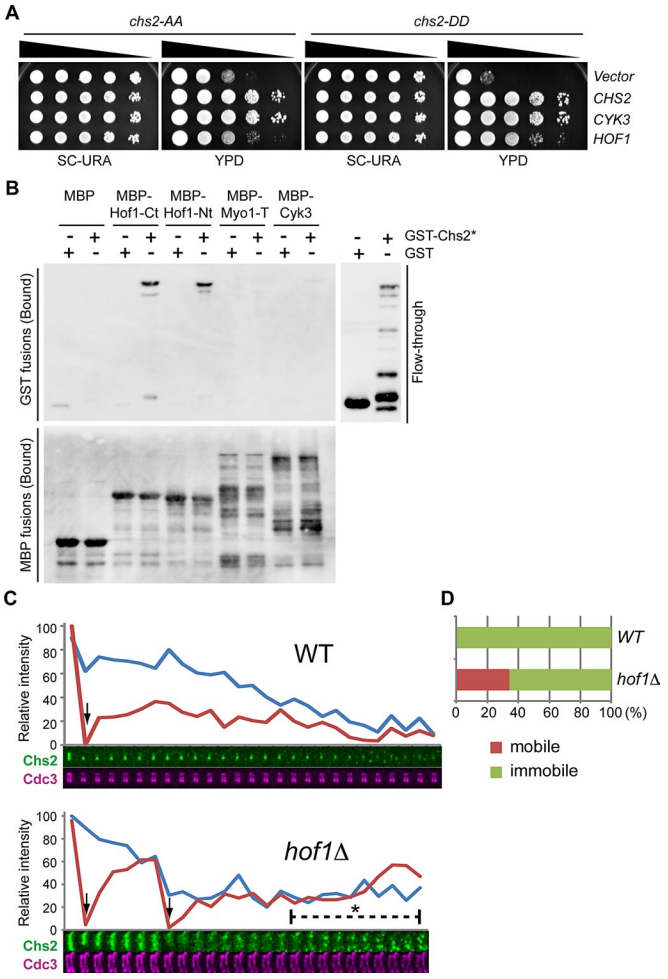

FIGURE 8: Hof1 interacts directly with Chs2, stabilizes it at the division site, and suppresses the cytokinesis defects of a *chs2* mutant. (A) Increased dose of Hof1 specifically suppresses the growth and cytokinesis defects of the *chs2-DD* but not the *chs2-AA* mutants. Tenfold serial dilutions of the *chs2-AA*– or *chs2-DD*–derived strains carrying a high-copy plasmid alone (Vector) or containing a specific gene (*CHS2*, *CYK3*, or *HOF1*) were spotted onto plates containing either minimal medium (SC-URA) or rich medium (YPD) and grown at 25°C for 2–3 d (the *chs2-AA*–derived strains: YO1543, Vector; YO1442, *CHS2*; YO1544, *CYK3*; and YO1545, *HOF1*. The *chs2-DD*–derived strains: YO1550, Vector; YO1443, *CHS2*; YO1551, *CYK3*; and YO1552, *HOF1*). (B) Both Hof1-N-term and Hof1-C-term bind to Chs2 in vitro. Recombinant MBP-Hof1 fragments (MBP-Hof1-Ct and MBP-Hof1-Nt), along with the controls (MBP, MBP-Myo1-tail, and MBP-Cyk3), were assessed for their interactions with a recombinant GST-Chs2 fragment containing a portion of its intracellular domain (GST-Chs2 (1-286)) or GST alone (control). (C) Chs2 becomes more mobile at the division site in *hof1Δ* cells. The wild-type (WT, YEF6653; top) and *hof1Δ* (YEF6654; bottom) cells carrying *CHS2-GFP* and *CDC3-mChery* were grown to the exponential phase in SC-HIS and then changed to YM-1 rich media for at least 3 additional hours of growth. The dynamics of Chs2 during cytokinesis in these strains was then analyzed by FRAP. Blue lines, fluorescence signal in the unbleached region; red lines, fluorescence signal in the bleached region; arrows, photobleaching point; asterisk, the period when endocytic vesicles carrying the Chs2-GFP cargoes linger around the division site, which complicates the quantitative analysis of fluorescence signal during that period. (D) Quantitative analysis of the fluorescence recovery patterns using the data acquired in C (WT, $n = 17$; *hof1Δ*, $n = 44$).

enriched phospholipids. The CC2 region localizes to the bud neck throughout the cell cycle by interacting with septin complexes. However, the F-BAR domain is clearly required for the efficient targeting of the CC2 region to the bud neck by promoting its cortical enrichment and/or by regulating its conformation, which enables a more robust interaction with septin complexes.

Hof1-C-term localizes to the bud neck shortly before the onset of cytokinesis and constricts together with the AMR like the full-length protein does. In addition, the localization of Hof1-C-term to the middle position between the septin rings during cytokinesis depends on Myo1. Furthermore, Hof1-C-term interacts directly with Myo1-tail in vitro. This interaction presumably accounts for the association of the full-length Hof1 with the AMR during cytokinesis. The Hof1–Myo1 interaction must also be regulated during the cell cycle, as both proteins localize to the division site long before the onset of cytokinesis and yet do not interact until the beginning of the division process. Indeed, Hof1 is phosphorylated by the Polo kinase Cdc5 and the mitotic exit kinase Dbf2-Mob1 (Meitinger *et al.*, 2011), which presumably enables the switch in Hof1 interaction from the septins to Myo1.

In summary, our study indicates that Hof1 contains three distinct targeting domains that confer distinct patterns of localization by interacting with different binding partners. Based on this and other studies, a clear picture of the mechanism of Hof1 localization and regulation during the cell cycle is beginning to emerge (Figure 9A). Hof1 is expressed in S/G2 (Vallen *et al.*, 2000), and its localization to

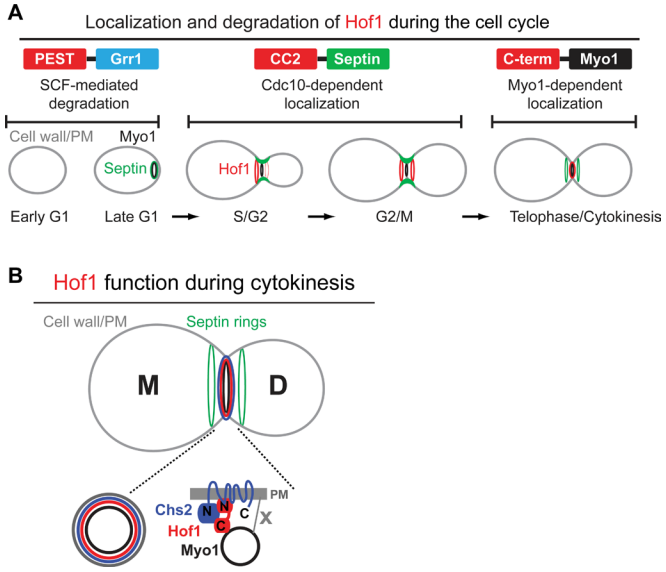

FIGURE 9: (A) A model for Hof1 localization and degradation during the cell cycle. From S/G2 to the end of mitosis, Hof1 is targeted to the bud neck by interacting with septin complexes in a Cdc10-dependent manner. This interaction is mediated by the N-terminus of Hof1, primarily through its CC2 region. From the onset of telophase to the end of cytokinesis, Hof1 colocalizes with the AMR through an interaction between its C-terminus and Myo1-tail. In the absence of Myo1, Hof1 interacts with the septin rings and the PM between the rings during cytokinesis. During and after cytokinesis, Hof1 is degraded through SCF-mediated degradation. See the text for details. (B) A model for Hof1 function in cytokinesis. Hof1 couples AMR constriction to PS formation by interacting with Myo1 and Chs2. D, daughter cell; M, mother cell; X, an unknown mechanism that links Myo1 to the PM. See the text for details.

the bud neck from this point to the onset of cytokinesis depends on its interaction with septin complexes. More specifically, this interaction requires the CC2 region of Hof1 and the septin subunit Cdc10. During the mitotic exit, Hof1 is phosphorylated (Vallen *et al.*, 2000; Blondel *et al.*, 2005; Meitinger *et al.*, 2011), leading to its release from the septins and its association with the AMR (Meitinger *et al.*, 2011). This Hof1–AMR association is mediated by an interaction between Hof1-C-term and Myo1-tail. During and immediately after cytokinesis, Hof1 undergoes SCF-mediated degradation, which requires the PEST sequence of Hof1 and the F-box protein Grr1 (Blondel *et al.*, 2005). The spatiotemporally controlled degradation of Hof1 is required for efficient AMR constriction and subsequent cell separation (Blondel *et al.*, 2005).

Hof1 couples actomyosin ring constriction with septum formation during cytokinesis

We propose that Hof1 couples AMR constriction to PS formation during cytokinesis by interacting with Myo1 and Chs2 (Figure 9B). This hypothesis is supported by multiple observations made in this study: 1) Hof1-C-term interacts directly with Myo1-tail; 2) the association between Hof1-C-term and the AMR during cytokinesis depends on Myo1; 3) both the N- and C-terminal regions of Hof1 interact directly with the intracellular domain of Chs2; 4) increased dosage of Hof1 suppresses the growth and cytokinesis defects of *chs2-DD* mutant, which is known to prematurely dissociate from the AMR (Oh *et al.*, 2012); and 5) deletion of *HOF1* does not affect Myo1 immobility (Wloka *et al.*, 2013) but destabilizes Chs2 during cytokinesis.

The role of Hof1 in cytokinesis may be more complex than simply acting as a linker between Myo1 and Chs2. The SH3 domain of Hof1 has been shown to interact with the proline-rich motifs in verprolin (Vrp1), the counterpart of the Wiskott–Aldrich syndrome protein (WASP)–interacting protein (WIP) in animal cells (Ren *et al.*, 2005). This interaction is believed to relieve an inhibitory effect of the SH3 domain on cytokinesis, which is consistent with our observation that overexpression of Hof1-C-term inhibited cytokinesis. Because Vrp1 plays an essential role in endocytosis (Munn *et al.*, 1995), the Vrp1–Hof1 interaction also suggests that the SH3 domain may regulate cytokinesis through endocytosis. This is unlikely, as we did not find an apparent defect in Myo1 ring constriction in cells lacking Las17/Bee1 (unpublished data), the yeast homologue of WASP that is required for endocytosis (Li, 1997; Madania *et al.*, 1999). However, this observation does not rule out the possibility that endocytosis may fine tune cytokinesis, especially septum formation by controlling the turnover of enzymatic cargoes such as Chs2 at the division site. The SH3 domain of Hof1 also interacts with Inn1, a protein required for PS formation (Nishihama *et al.*, 2009; Labedzka *et al.*, 2012). As discussed earlier, this interaction may account for the role of the SH3 domain in maintaining the symmetry of Myo1 ring constriction during cytokinesis.

Like Hof1, most F-BAR proteins contain an F-BAR domain at their N-termini and an SH3 domain at the C-termini (Heath and Insall, 2008; Suetsugu *et al.*, 2010). These proteins are best known to function in clathrin-mediated endocytosis by coupling actin and membrane dynamics. In the fission yeast *Schizosaccharomyces pombe*, the F-BAR protein Cdc15 plays an essential role in cytokinesis by acting as a scaffold that interacts with multiple proteins involved in cytokinesis, including the formin (Cdc12 in fission yeast), myosin-I (Myo1 in fission yeast, an activator of the Arp2/3 complex), IQGAP (Rng2), Fic1, and Cyk3 (Carnahan and Gould, 2003; Roberts-Galbraith *et al.*, 2009, 2010; Roberts-Galbraith and Gould, 2010). These binding partners play distinct roles in AMR assembly and/or septum formation. In mammalian cells, the F-BAR protein PSTPIP1 (proline, serine, threonine phosphatase–interacting protein) localizes to the cleavage furrow and the cell cortex and participates in cytokinesis and other cellular processes (Spencer *et al.*, 1997; Wu *et al.*, 1998; Angers-Loustau *et al.*, 1999; Heath and Insall, 2008). Because of the complexity involved in their interactions with multiple binding partners and the spatiotemporal control of these interactions, it has been a challenge to understand the detailed mechanism underlying the role of F-BAR proteins in cytokinesis. It also remains to be seen whether F-BAR proteins in different organisms function in cytokinesis through some common mechanisms.

In this study, we determined the comprehensive mechanism underlying Hof1 targeting to the division site, which explains the complex localization pattern of Hof1 during the cell cycle. In addition, we presented evidence to suggest that Hof1 functions in cytokinesis by coupling AMR constriction to PS formation. Although there are a number of open questions regarding the role of Hof1 in cytokinesis, this study will contribute to an understanding of how F-BAR proteins might function in diverse cellular processes by acting as cortical organizers that link the PM to a cytoskeleton-based machine.

MATERIALS AND METHODS

Strains, growth conditions, and genetic methods

The yeast strains used in this study are listed in Table 1. Standard culture media and genetic methods were used (Guthrie and Fink, 1991). *E. coli* strains DH12S (Invitrogen, Carlsbad, CA) and BL21 (DE3; Invitrogen) were used as hosts for plasmid manipulation and recombinant protein expression, respectively. Yeast strains were grown

Strain	Genotype	Source
YEF473	**a**/α *his3/his3 leu2/leu2 lys2/lys2 trp1/trp1 ura3/ura3*	Bi and Pringle (1996)
YEF473A	**a** *his3 leu2 lys2 trp1 ura3*	Bi and Pringle (1996)
YEF473B	α *his3 leu2 lys2 trp1 ura3*	Bi and Pringle (1996)
YEF1951	**a** *hof1Δ::KanMX6*	Vallen *et al*. (2000)
YEF2680	**a** *hof1Δ::KanMX6 cyk3Δ::HIS3* [pRS316-HOF1]	This study[a]
YEF4551	**a** *hof1Δ::KanMX6* [YCp50-LEU2-HOF1-GFP::KanMX6]	This study
YEF4552	**a** *hof1Δ::KanMX6* [YCp50-LEU2-Hof1-SH3Δ (1-602)-GFP::KanMX6]	This study
YEF4554	**a** *hof1Δ::KanMX6* [YCp50-LEU2-Hof1-N-term (1-340)-GFP::KanMX6]	This study
YEF4600	**a** *hof1Δ::TRP1*	This study
YEF4909	**a** *hof1Δ::KanMX6* [YCp50-LEU2]	This study
YEF4911	**a** *hof1Δ::KanMX6* [pRS315-Hof1-PESTΔ (418-438)-GFP::KanMX6]	This study
YEF4913	**a** *hof1Δ::KanMX6* [pRS315-Hof1-C-term (341-669)-GFP::KanMX6]	This study
YEF4944	**a** *hof1Δ::KanMX6 cyk3Δ::HIS3* [pRS316-HOF1] [YCp50-LEU2-Hof1-SH3Δ (1-602)::TRP1]	This study
YEF4945	**a** *hof1Δ::KanMX6 cyk3Δ::HIS3* [pRS316-HOF1] [YCp50-LEU2- HOF1-N-term (1-340)::TRP1]	This study
YEF4948	**a** *hof1Δ::KanMX6 cyk3Δ::HIS3* [pRS316-HOF1] [pRS315-Hof1-PESTΔ (418-438)]	This study
YEF4949	**a** *hof1Δ::KanMX6 cyk3Δ::HIS3* [pRS316-HOF1] [pRS315-Hof1- C-term (341-669)]	This study
YEF4966	**a** *hof1Δ::KanMX6 cyk3Δ::HIS3* [pRS316-HOF1] [YCp50-LEU2-HOF1]	This study
YEF4970	**a** *hof1Δ::KanMX6 cyk3Δ::HIS3* [pRS316-HOF1] [YCp50-LEU2]	This study
YEF5421	**a** *hof1Δ::TRP1 CDC3-mCherry::URA3* [YCp50-LEU2-Hof1-N-term (1-340)-GFP::KanMX6]	This study
YEF5422	**a** *CDC3-mCherry::URA3* [YCp50-LEU2-Hof1-C-term (341-669)-GFP::KanMX6]	This study
YEF5423	**a** *hof1Δ::TRP1 CDC3-mCherry::URA3* [YCp50-LEU2-Hof1-C-term (341-669)-GFP::KanMX6]	This study
YEF5451	**a** *hof1Δ::TRP1 myo1Δ::HIS3* [YCp50-MYO1]	This study
YEF5479	**a** *hof1Δ::TRP1 CDC3-mCherry::URA3* [YCp50-LEU2-HOF1-GFP::KanMX6]	This study
YEF5812	**a**/α *HIS3-pCET1-Vc-HOF1/HOF1 CDC3-Vn::TRP1/CDC3* [YCp111-CDC3]	This study
YEF5813	**a**/α *HIS3-pCET1-Vc-HOF1/HOF1 CDC10-Vn::KanMX6/CDC10*	This study
YEF5814	**a**/α *HIS3-pCET1-Vc-HOF1/HOF1 CDC11-Vn::TRP1/CDC11*	This study
YEF5815	**a**/α *HIS3 pCET1-Vc-HOF1/HOF1 CDC12-Vn::TRP1/CDC12* [pRS316-CDC12]	This study
YEF5816	**a**/α *HIS3-pCET1-Vc-HOF1/HOF1 SHS1-Vn::TRP1/SHS1*	This study
YEF5881	**a**/α *HIS3-pCET1-Vc-Hof1-N-term (1-340)::KanMX6 /HOF1 CDC10-Vn::KanMX6/CDC10*	This study
YEF5883	**a**/α *HIS3-pCET1-Vc-Hof1-N-term (1-340)::KanMX6 /HOF1 CDC3-Vn::TRP1/CDC3* [YCp111-CDC3]	This study
YEF5884	**a**/α *HIS3-pCET1-Vc-Hof1-N-term (1-340)::KanMX6 /HOF1 CDC11-Vn::TRP1*	This study
YEF5885	**a**/α *HIS3-pCET1-Vc-Hof1-N-term (1-340)::KanMX6 /HOF1 CDC12-Vn::TRP1/CDC12* [pRS316-CDC12]	This study
YEF5886	**a**/α *HIS3-pCET1-Vc-Hof1-N-term (1-340)::KanMX6 /HOF1 SHS1-Vn::TRP1/SHS1*	This study
YEF5930	**a**/α *HIS3-pCET1-Vc-Hof1-C-term (341-669) /HOF1 CDC3-Vn::TRP1/CDC3* [YCp111-CDC3]	This study
YEF5931	**a**/α *HIS3-pCET1-Vc-Hof1-C-term (341-669) /HOF1 CDC11-Vn::KanMX6/CDC11*	This study
YEF5932	**a**/α *HIS3-pCET1-Vc-Hof1-C-term (341-669) /HOF1 CDC12-Vn::TRP1/CDC12* [pRS316-CDC12]	This study
YEF5933	**a**/α *HIS3-pCET1-Vc-Hof1-C-term (341-669) /HOF1 SHS1-Vn::TRP1/SHS1*	This study
YEF5934	**a**/α *HIS3-pCET1-Vc-Hof1-C-term (341-669) /HOF1 CDC10-Vn::KanMX6/CDC10*	This study
YEF6383	α *chs2Δ::HIS3 CDC3-mCherry::TRP1* [pRS315-Hof1-C-term (341-669)-GFP::KanMX6]	This study
YEF6392	**a** *myo1Δ::KanMX6 CDC3-mCherry::TRP1* [pRS315-Hof1-C-term (341-669)-GFP::KanMX6]	This study
YEF6532	**a** *cdc10Δ::KanMX6 CDC3-mCherry::TRP1* [pRS315-Hof1-N-term (1-340)-GFP::KanMX6]	This study
YEF6653	**a** *CHS2-GFP::HIS3 CDC3-mCherry::URA3*	This study
YEF6654	**a** *hof1Δ::TRP1 CHS2-GFP::HIS3 CDC3-mCherry::URA3*	This study

TABLE 1: Yeast strains used in this study.

Continues

Strain	Genotype	Source
YO1442	α *chs2Δ::HIS3 CDC3-mCherry::TRP1 Chs2 (S217A S225A)-GFP::KanMX6* + [pEC2 (*CHS2, URA3, 2μ*)]	This study
YO1443	α *chs2Δ::HIS3 CDC3-mCherry::TRP1 Chs2 (S217D S225D)-GFP::KanMX6* + [pEC2 (*CHS2, URA3, 2μ*)]	This study
YO1473	**a** *cdc10Δ::KanMX6 CDC3-mCherry::TRP1* [pRS315-Hof1-C-term (341-669)-GFP::KanMX6]	This study
YO1538	**a** *shs1Δ::KanMX6 CDC3-mCherry::TRP1* [YCp50- LEU2-Hof1-N-term (1-340)-GFP::KanMX6]	This study
YO1542	**a** *cdc11Δ::TRP1 Cdc3-mCherry::URA3* [YCp50- LEU2-Hof1-N-term (1-340)-GFP::KanMX6]	This study
YO1543	α *chs2Δ::HIS3 CDC3-mCherry::TRP1 Chs2 (S217A S225A)-GFP::KanMX6* [pAG426, *2μ, URA3*]	Oh *et al.* (2012)
YO1544	α *chs2Δ::HIS3 CDC3-mCherry::TRP1 Chs2 (S217A S225A)-GFP::KanMX6* [pAG426-CYK3, *2μ, URA3*]	Oh *et al.* (2012)
YO1545	α *chs2Δ::HIS3 CDC3-mCherry::TRP1 Chs2 (S217A S225A)-GFP::KanMX6* [pAG426-HOF1, *2μ, URA3*]	This study
YO1550	α *chs2Δ::HIS3 CDC3-mCherry::TRP1 Chs2 (S217D S225D)-GFP::KanMX6* [pAG426, *2μ, URA3*]	Oh *et al.* (2012)
YO1551	α *chs2Δ::HIS3 CDC3-mCherry::TRP1 Chs2 (S217D S225D)-GFP::KanMX6* [pAG426-CYK3, *2μ, URA3*]	Oh *et al.* (2012)
YO1552	α *chs2Δ::HIS3 CDC3-mCherry::TRP1 Chs2 (S217D S225D)-GFP::KanMX6* [pAG426-HOF1, *2μ, URA3*]	This study
YO1834	**a** *KanMX6-pGal1-Hof1-N-term (1-340)::HIS3 CDC3-mCherry::LEU2*	This study
YO1847	**a** *KanMX6-pGal1-Hof1-C-term (341-669) CDC3-mCherry::LEU2* [pRS316-Myo1-C-GFP]	This study
YO1860	**a** *CDC3-mCherry::LEU2* [pRS316-Myo1-C-GFP]	This study
YO1864	**a** *hof1Δ::NatMX6 CDC3-mCherry::TRP1* [pRS316-Myo1-C-GFP]	This study
YO1870	**a** *KanMX6-pGal1-Hof1-C-term-SH3Δ (341-601) CDC3-mCherry::LEU2* [pRS316-Myo1-C-GFP]	This study
YO1875	**a** *KanMX6-pGal1-Hof1-F-BAR (1-275)::HIS3 CDC3-mCherry::Leu2*	This study
YO1878	**a** *hof1Δ::NatMX6 CDC3-mCherry::TRP1* [YCp50-LEU2-Hof1-CC2 (276-340)::GFP::KanMX6]	This study
YO1879	**a** *hof1Δ::NatMX6 CDC3-mCherry::TRP1* [YCp50-LEU2-Hof1-F-BAR (1-275)::GFP::KanMX6]	This study
YO1880	**a** *hof1-F-BAR (1-275)::GFP::KanMX6 CDC3-mCherry::LEU2*	This study
YO1947	**a** *hof1Δ::TRP1 myo1Δ::HIS3* [YCp50-MYO1] [pRS315]	This study
YO1948	**a** *hof1Δ::TRP1 myo1Δ::HIS3* [YCp50-MYO1] [pRS315-HOF1]	This study
YO1949	**a** *hof1Δ::TRP1 myo1Δ::HIS3* [YCp50-MYO1] [pRS315-Hof1-C-term]	This study
YO1950	**a** *hof1Δ::TRP1 myo1Δ::HIS3* [YCp50-MYO1] [YCp50-LEU2-Hof1-SH3Δ]	This study
YO1966	**a** *hof1Δ::NatMX6 CDC3-mCherry::TRP1* [pRS316-Myo1-C-GFP] [pRS315-HOF1]	This study
YO1967	**a** *hof1Δ::NatMX6 CDC3-mCherry::TRP1* [pRS316-Myo1-C-GFP] [YCp50-LEU2-Hof1-SH3Δ]	This study
YO1972	**a** *hof1Δ::KanMX6 cyk3Δ::HIS3* [pRS316-HOF1] [pRS315-Hof1- CC2Δ]	This study
YO1973	**a** *hof1Δ::TRP1 myo1Δ::HIS3* [YCp50-MYO1] [pRS315-Hof1- CC2Δ]	This study
YO1974	**a** *hof1Δ::TRP1 CDC3-mCherry::URA3* [pRS315-Hof1-CC2Δ-GFP::KanMX6]	This study

[a]All other YEF strains and all the YO strains are derived from YEF473, YEF473A, or YEF473B.

TABLE 1: Yeast strains used in this study. Continued

routinely at 25°C in synthetic complete (SC) minimal medium lacking specific amino acid(s) and/or uracil or in rich medium YM-1 (Lillie and Pringle, 1980) or yeast/peptone/dextrose (YPD). In some experiments, 1 mg/ml 5-FOA (Research Products International, Mt. Prospect, IL) was added to media to select for the loss of *URA3*-containing plasmids. To depolymerize F-actin (Ayscough *et al.*, 1997), LatA (Wako Chemicals USA, Richmond, VA) dissolved in dimethyl sulfoxide (DMSO) was added to cell cultures to a final concentration of 200 μM. Oligonucleotide primers were purchased from Integrated DNA Technologies (Coralville, IA).

Constructions of plasmids and yeast strains

Commonly used plasmid vectors in this study are YCp50-LEU2 (*CEN*, *LEU2*; Bi and Pringle, 1996) and pRS315 (*CEN*, *LEU2*; Sikorski and Hieter, 1989). The plasmids pEC2 (*2μ*, *CHS2, URA3*; Ford *et al.*, 1996), pRS316-HOF1 (*CEN, HOF1, URA3*; Vallen *et al.*, 2000), YCp50-LEU2-HOF1 (*CEN, HOF1, LEU2*; Nishihama *et al.*, 2009), and pRS316-MYO1-C-GFP (*CEN, URA3*; Fang *et al.*, 2010) were described previously. Plasmids YIplac128-CDC3-mCherry (integrative, *LEU2*; Gao *et al.*, 2007), YIplac211-CDC3-mCherry (integrative, *URA3*; Fang *et al.*, 2010), and YIplac204-CDC3-mCherry (integrative, *TRP1*; Wloka *et al.*, 2011), carrying *mCherry*-tagged *CDC3*, were digested with *Bgl*II and integrated at the *CDC3* locus of the recipient strains. Plasmid pRS315-HOF1 was constructed by subcloning an *Xba*I-digested, 5-kb fragment containing *HOF1* from YCp50-LEU2-HOF1 into the corresponding site of pRS315. Plasmids YCp50-LEU2-Hof1-N-term (1-340)::TRP1 and YCp50-LEU2-Hof1-SH3Δ(1-601)::TRP1 were constructed by a PCR-based approach (Longtine *et al.*, 1998), directly inserting a STOP codon after the codon 340 or 601of *HOF1* carried on the plasmid YCp50-LEU2-HOF1 in a *hof1Δ::KanMX6* strain. Plasmids pRS315-Hof1-C-term (341-669), pRS315-Hof1-CC2Δ (276-340)Δ, and pRS315-Hof1-PESTΔ (418-438)Δ were constructed by a PCR-based deletion method using pRS315-HOF1 as the template.

Plasmids YCp50-LEU2-HOF1-GFP::KanMX6, YCp50-LEU2-Hof1-N-term-GFP::KanMX6, YCp50-LEU2-Hof1-SH3Δ-GFP::KanMX6, pRS315-Hof1-PESTΔ-GFP::KanMX6, YCp50-LEU2-Hof1-F-BAR-GFP::KanMX6, pRS315-Hof1-CC2Δ-GFP::KanMX6, and pRS315-Hof1-C-term-GFP::KanMX6 were constructed by PCR-based C-terminal tagging of *HOF1* or its fragment carried on plasmid YCp50-LEU2-HOF1 or its derivative using *GFP-KanMX6* fragment amplified from the plasmid pFA6a-GFP-kanMX6 (Longtine *et al.*, 1998). Plasmid YCp50-LEU2-Hof1-CC2 (276-340)-GFP::KanMX6 was constructed by PCR-based deletion of an appropriate region in YCp50-LEU2-N-term-GFP::KanMX6. Plasmids pMAL-C2-Hof1, -Hof1-N-term (1-340), -Hof1-C-term (341-669), Hof1-F-BAR (1-275), Hof1-CC2 (276-340), and -Cyk3 were constructed by cloning a *Bam*HI and *Sal*I (both sites introduced in PCR primers)–digested *HOF1* fragment or *CYK3* into the corresponding sites of pMAL-C2 (New England BioLabs, Ipswich, MA). Plasmids pMAL-C2- Myo1-tail (856-1928), pMAL-C2-TD1 (856-1253, 1398-1928), and pMAL-C2-Myo1-TD2 (1254-1397) were described previously (Fang *et al.*, 2010). Plasmid pGEX5X-1-Hof1-C-term was constructed by cloning a *Bam*HI and *Sal*I–digested *hof1-C-term* fragment into the corresponding sites of pGEX5X-1 (GE Healthcare, Pittsburgh, PA).

The *KanMX6-pGAL1-HOF1* and *KanMX6-pGAL1-Hof1-C-term* strains were constructed by inserting a 2.0-kb PCR fragment containing *KanMX6-pGAL1* (Longtine *et al.*, 1998) in front of either the START codon or the codon 341 of *HOF1* on the chromosome. The *KanMX6-pGAL1-Hof1-N-term::HIS3MX6* and *KanMX6-pGAL1-Hof1-F-BAR::HIS3MX6* strains were constructed by a PCR-based method (Longtine *et al.*, 1998), directly inserting a STOP codon after the codon 340 or 275 of *HOF1* on the chromosome of the strain *KanMX6-pGAL1-HOF1*. Similarly, the *KanMX6-pGAL1-Hof1-C-term-SH3Δ(341-601)::HIS3MX6* strain was constructed by inserting a STOP codon after the codon 601 of *HOF1* on the chromosome of the strain *KanMX6-pGAL1-Hof1-C-term*. Plasmid pAG24-HOF1 was constructed by transferring *HOF1* from the targeting-induced local lesions in genomes (TILLING) library plasmid pGP564-HOF1 (*2*μ, *LEU2*; Open Biosystems, Lafayette, CO) onto the Gateway vector pAG24 (*2*μ, *URA3*) using Gateway LR Clonase II (Invitrogen, Grand Island, NY).

Bimolecular fluorescence complementation assay

Yeast strains used for the BiFC assay (Hu *et al.*, 2002) were constructed by a PCR-based approach (Sung and Huh, 2007). For one set of strains, the last codon of each septin gene (*CDC3*, *CDC10*, *CDC11*, *CDC12*, *SHS1*) at its physiological locus was directly fused in-frame with the N-terminal fragment of Venus (Vn), a variant of the yellow fluorescence protein, respectively, in a MAT**a** strain (YEF473A). In case of *CDC3* and *CDC12*, due to the sickness of the resulting strains, a supporting plasmid YCplac111-CDC3 (*CEN*, *LEU2*) or pRS316-CDC12 (*CEN*, *URA3*; both plasmids were kindly supplied by M. Longtine, Washington University, St. Louis, MO) was transformed into YEF473A before the chromosomal tagging. For the second set of strains, a PCR fragment containing the *pCET1* promoter and the C-terminal fragment of Venus (Vc) was directly inserted in-frame before the START codon of *HOF1*, *hof1-N-term*, or *hof1-C-term* on the chromosome of an appropriate MATα strain (YEF473B or its derivative). After pairwise mating between the two sets of strains, diploids were selected on either SC-HIS-TRP plates or SC-HIS plates containing 200 μg/ml G418. Fluorescence signals from the diploid cells were observed using the spinning-disk confocal microscope system (see later description).

Microscopy

A computer-controlled Eclipse 800 microscope (Nikon, Tokyo, Japan) and a high-resolution charge-coupled device (CCD) camera (model C4742-95; Hamamatsu Photonics, Bridgewater, NJ) were used to visualize cell morphologies by differential interference contrast microscopy. The images were acquired using Image-Pro Plus, version 7.0 (Media Cybernetics, Bethesda, MD). For live-cell imaging of yeast strains carrying a plasmid, cells were grown at 25°C in SC media lacking a specific amino acid to select for the presence of a plasmid. For imaging yeast strains carrying a *hof1* fragment under the control of the *pGAL1* promoter, cells were first grown in the rich medium YM-1 containing 2% galactose and 2% raffinose. Cells were then concentrated by centrifugation and spotted on a slab of YM-1 medium containing 2% galactose, 2% raffinose, and 2% agarose for live-cell imaging. Images were acquired at 25°C on a spinning-disk confocal microscope equipped with a Yokogawa CSU 10 scan head (Yokogawa, Tokyo, Japan) combined with an Olympus IX 71 microscope and an Olympus 100× objective (1.4 numerical aperture, Plan S-Apo oil immersion; Olympus, Tokyo, Japan). Acquisition and hardware were controlled by MetaMorph, version 7.7 (Molecular Devices, Downingtown, PA). A Hamamatsu ImagEM electron-multiplying CCD camera (model C9100-13; Hamamatsu Photonics) was used for image capture. Diode lasers for excitation (488 nm for GFP and 561 nm for mCherry/RFP) were housed in a launch constructed by Spectral Applied Research (Richmond Hill, Canada). Images were taken every minute with *z*-stacks ranging from 11 × 0.3 to 11 × 0.5 μm. Maximum projections were generated with MetaMorph, version 7.7 (Molecular Devices, Downingtown, PA) or ImageJ (1.45b; National Institutes of Health, Bethesda, MD). For the experiments involving FRAP, cells were grown to exponential phase in SC-HIS media at 23°C. Cells were then centrifuged and resuspended in 10 ml YM-1 medium and grown for at least another 3 h in a 50-ml flask at 25°C in a water-bath shaker. One milliliter of this culture was taken to concentrate the cells by centrifugation. Cells were then spotted on YM-1 medium containing 2% agarose for FRAP and imaging analysis. FRAP was performed using a MicroPoint computer-controlled ablation system (Photonic Instruments, St. Charles, IL) consisting of a nitrogen-pumped dye laser (wavelength, 435 nm) controlled by MetaMorph. In some cases, sequential photobleaching was applied. Images were captured and processed using the same microscope, camera, and software as described. Images were taken every 20 s with a *z*-stack consisting of 12 × 0.4–μm optical sections.

In vitro binding experiment

To purify the five-septin complexes, *E. coli* strain BL21 (DE3) (Invitrogen) containing pMVB128 (expressing Cdc10 and His_6-Cdc12; ampicillin resistant), pMVB133 (expressing Cdc3 and Cdc11; chloramphenicol resistant), and pCOLA-Duet-Shs1 (expressing Shs1; kanamycin resistant), kindly provided by J. Thorner (University of California, Berkeley, CA; Versele *et al.*, 2004; Garcia *et al.*, 2011), was grown to exponential phase at 37°C, and protein expression was induced with the addition of 1 mM isopropyl-β-D-thiogalactoside for 3 h at 23°C. The four-septin complexes were expressed from the BL21 (DE3) containing pMVB128 (Cdc10 and His_6-Cdc12) and pMVB133 (Cdc3 and Cdc11). The three-septin complexes were expressed from plasmids pMVB133 (Cdc3 and Cdc11) and pMVB12-Cdc12–His_6. To purify the septin complexes, cells were resuspended with nickel-nitriloacetic acid (Ni-NTA) lysis buffer (300 mM NaCl, 5 mM $MgCl_2$, 20 mM Tris-HCl, pH 8.0, 20 mM imidazole, 10 mM β-mercaptoethanol, 0.1% NP-40) containing a cocktail of protease inhibitors (Roche, Indianapolis, IN). Cells were then sonicated six times

with 40 amplitude (QSonica Q55, Newtown, CT) for 15 s with 1-min interval on ice. The protein extracts were centrifuged at 13,500 rpm for 20 min at 4°C. The supernatant was mixed with Ni-NTA beads (Qiagen, Valencia, CA) that had been freshly washed three times with Ni-NTA lysis buffer. After rocking for 2 h at 4°C, the beads were centrifuged at 3000 rpm for 10 s, then washed three times with Ni-NTA buffer. Septin complexes were then eluted four times with freshly prepared elution buffer (300 mM NaCl, 5 mM $MgCl_2$, 20 mM Tris-HCl, pH 8.0, 300 mM imidazole, 10 mM β-mercaptoethanol, 0.1% NP-40).

To purify MBP- and glutathione *S*-transferase (GST)–tagged proteins, *E. coli* BL21 (DE3) was transformed with pGEX-5X-based plasmids or pMAL-C2-based plasmids (see prior description). The tagged proteins were purified following the protocols described previously (Fang *et al.*, 2010).

For the in vitro binding experiments, the elution buffer in which the septin complexes were dissolved was exchanged to the binding buffer (300 mM NaCl, 5 mM $MgCl_2$, 20 mM Tris-HCl, pH 8.0, 10 mM β-mercaptoethanol, 0.1% NP-40) using centrifugal filters (Amicon Ultra 10,000 MWCO; Millipore, Billerica, MA). To adjust salt concentration in the septin complexes to 100 mM NaCl, two volumes of the binding buffer without NaCl was added to one volume of septin complexes in the binding buffer with 300 mM NaCl and then incubated for 1 h at 4°C. Approximately 20 µg of MBP-tagged proteins bound on amylose beads, whose volume was normalized by adding prewashed amylose beads, were mixed with 5 µg of five-, four-, or three-septin complexes. The mixtures were incubated with rotation for 1 h at 4°C and then pelleted by centrifugation. The pellets were washed with 1 ml of the same binding buffer (100 mM NaCl or 300 mM NaCl). A 2× SDS sample buffer (Santa Cruz Biotechnology, Santa Cruz, CA) was then added to the beads, which were boiled for 5 min. Proteins were resolved by SDS–PAGE and analyzed by Western blotting using rabbit polyclonal antibodies against Cdc11 (Santa Cruz Biotechnology). The in vitro binding experiments between MBP-tagged and GST-tagged proteins were performed following the protocol described previously (Fang *et al.*, 2010).

Protein extraction and Western blotting

Cells were grown in appropriate media to select for the presence of the plasmid at 25°C overnight. Then 10 ml of the cells were pelleted and resuspended with 500 µl of 20% trichloroacetic acid. Cells were then lysed by beating with acid-washed glass beads (Sigma-Aldrich, St. Louis, MO) in a Bead Beater (MiniBeadBeater-16; Biospec Products, Bartlesville, OH) for six cycles of 30-s beating and 1-min chilling on ice. Cell lysates were centrifuged and resuspended in 100 µl of 1× phosphate-buffered saline buffer containing 0.1% NP-40 and then mixed with 20 µl of 6× sample buffer; this was then neutralized with 1 N NaOH and boiled for 5 min. Proteins were resolved by SDS–PAGE and analyzed by Western blotting using the mouse anti-GFP (1:10,000, MMS-118P; Covance, Berkeley, CA) and the goat anti-Cdc28 (1:2000, yC-20; Santa Cruz Biotechnology) antibodies. The secondary antibodies were anti-mouse immunoglobulin G (IgG; 1:10,000) and anti-goat IgG (1:10,000) conjugated to horseradish peroxidase (Jackson ImmunoResearch Laboratories, West Grove, PA).

ACKNOWLEDGMENTS

We thank G. Pereira, K. Moravcevic, and M. Lemmon for sharing unpublished information; S. Okada and A. Stout for assistance with imaging;. W.-K. Huh and J. Thorner for plasmids; and the members of the Bi laboratory for discussions. This work was supported by National Institutes of Health Grants GM59216 and GM87365 (to E.B.) and a fellowship from the Boehringer Ingelheim Fonds (to C. W.).

REFERENCES

Angers-Loustau A, Cote JF, Charest A, Dowbenko D, Spencer S, Lasky LA, Tremblay ML (1999). Protein tyrosine phosphatase-PEST regulates focal adhesion disassembly, migration, and cytokinesis in fibroblasts. J Cell Biol 144, 1019–1031.

Ayscough KR, Stryker J, Pokala N, Sanders M, Crews P, Drubin DG (1997). High rates of actin filament turnover in budding yeast and roles for actin in establishment and maintenance of cell polarity revealed using the actin inhibitor latrunculin-A. J Cell Biol 137, 399–416.

Balasubramanian MK, Bi E, Glotzer M (2004). Comparative analysis of cytokinesis in budding yeast, fission yeast and animal cells. Curr Biol 14, R806–818.

Barr FA, Gruneberg U (2007). Cytokinesis: placing and making the final cut. Cell 131, 847–860.

Bi E (2001). Cytokinesis in budding yeast: the relationship between actomyosin ring function and septum formation. Cell Struct Funct 26, 529–537.

Bi E, Maddox P, Lew DJ, Salmon ED, McMillan JN, Yeh E, Pringle JR (1998). Involvement of an actomyosin contractile ring in *Saccharomyces cerevisiae* cytokinesis. J Cell Biol 142, 1301–1312.

Bi E, Pringle JR (1996). *ZDS1* and *ZDS2*, genes whose products may regulate Cdc42p in *Saccharomyces cerevisiae*. Mol Cell Biol 16, 5264–5275.

Blondel M, Bach S, Bamps S, Dobbelaere J, Wiget P, Longaretti C, Barral Y, Meijer L, Peter M (2005). Degradation of Hof1 by SCF(Grr1) is important for actomyosin contraction during cytokinesis in yeast. EMBO J 24, 1440–1452.

Boyne JR, Yosuf HM, Bieganowski P, Brenner C, Price C (2000). Yeast myosin light chain, Mlc1p, interacts with both IQGAP and class II myosin to effect cytokinesis. J Cell Sci 113, 4533–4543.

Carnahan RH, Gould KL (2003). The PCH family protein, Cdc15p, recruits two F-actin nucleation pathways to coordinate cytokinetic actin ring formation in *Schizosaccharomyces pombe*. J Cell Biol 162, 851–862.

Chin CF, Bennett AM, Ma WK, Hall MC, Yeong FM (2011). Dependence of Chs2 ER export on dephosphorylation by cytoplasmic Cdc14 ensures that septum formation follows mitosis. Mol Biol Cell 23, 45–58.

Chuang JS, Schekman RW (1996). Differential trafficking and timed localization of two chitin synthase proteins, Chs2p and Chs3p. J Cell Biol 135, 597–610.

Dobbelaere J, Barral Y (2004). Spatial coordination of cytokinetic events by compartmentalization of the cell cortex. Science 305, 393–396.

Epp JA, Chant J (1997). An IQGAP-related protein controls actin-ring formation and cytokinesis in yeast. Curr Biol 7, 921–929.

Fang X, Luo J, Nishihama R, Wloka C, Dravis C, Travaglia M, Iwase M, Vallen EA, Bi E (2010). Biphasic targeting and cleavage furrow ingression directed by the tail of a myosin-II. J Cell Biol 191, 1333–1350.

Ford RA, Shaw JA, Cabib E (1996). Yeast chitin synthases 1 and 2 consist of a non-homologous and dispensable N-terminal region and of a homologous moiety essential for function. Mol Gen Genet 252, 420–428.

Frazier JA, Wong ML, Longtine MS, Pringle JR, Mann M, Mitchison TJ, Field C (1998). Polymerization of purified yeast septins: evidence that organized filament arrays may not be required for septin function. J Cell Biol 143, 737–749.

Gao XD, Sperber LM, Kane SA, Tong Z, Hin Yan Tong A, Boone C, Bi E (2007). Sequential and distinct roles of the cadherin domain-containing protein Axl2p in cell polarization in yeast cell cycle. Mol Biol Cell 18, 2542–2560.

Garcia G 3rd, Bertin A, Li Z, Song Y, McMurray MA, Thorner J, Nogales E (2011). Subunit-dependent modulation of septin assembly: budding yeast septin Shs1 promotes ring and gauze formation. J Cell Biol 195, 993–1004.

Gladfelter AS, Pringle JR, Lew DJ (2001). The septin cortex at the yeast mother-bud neck. Curr Opin Microbiol 4, 681–689.

Guthrie C, Fink GR (1991). Guide to Yeast Genetics and Molecular Biology, San Diego, CA: Academic Press.

Hartwell LH (1971). Genetic control of the cell division cycle in yeast. IV. Genes controlling bud emergence and cytokinesis. Exp Cell Res 69, 265–276.

Heath RJ, Insall RH (2008). F-BAR domains: multifunctional regulators of membrane curvature. J Cell Sci 121, 1951–1954.

Hu CD, Chinenov Y, Kerppola TK (2002). Visualization of interactions among bZIP and Rel family proteins in living cells using bimolecular fluorescence complementation. Mol Cell 9, 789–798.

Itoh T, Erdmann KS, Roux A, Habermann B, Werner H, De Camilli P (2005). Dynamin and the actin cytoskeleton cooperatively regulate plasma membrane invagination by BAR and F-BAR proteins. Dev Cell 9, 791–804.
Kamei T, Tanaka K, Hihara T, Umikawa M, Imamura H, Kikyo M, Ozaki K, Takai Y (1998). Interaction of Bnr1p with a novel Src Homology 3 domain-containing Hof1p implication in cytokinesis in *Saccharomyces cerevisiae*. J Biol Chem 273, 28341–28345.
Kerppola TK (2008). Bimolecular fluorescence complementation (BiFC) analysis as a probe of protein interactions in living cells. Annu Rev Biophys 37, 465–487.
Korinek WS, Bi E, Epp JA, Wang L, Ho J, Chant J (2000). Cyk3, a novel SH3-domain protein, affects cytokinesis in yeast. Curr Biol 10, 947–950.
Labedzka K, Tian C, Nussbaumer U, Timmermann S, Walther P, Muller J, Johnsson N (2012). Sho1p connects the plasma membrane with proteins of the cytokinesis network via multiple isomeric interaction states. J Cell Sci 125, 4103–4113.
Li R ((1997). Bee1, a yeast protein with homology to Wiscott-Aldrich syndrome protein, is critical for the assembly of cortical actin cytoskeleton. J Cell Biol 136, 649–658.
Lillie SH, Pringle JR (1980). Reserve carbohydrate metabolism in *Saccharomyces cerevisiae*: responses to nutrient limitation. J Bacteriol 143, 1384–1394.
Lippincott J, Li R (1998a). Sequential assembly of myosin II, an IQGAP-like protein, and filamentous actin to a ring structure involved in budding yeast cytokinesis. J Cell Biol 140, 355–366.
Lippincott J, Li R (1998b). Dual function of Cyk2, a cdc15/PSTPIP family protein, in regulating actomyosin ring dynamics and septin distribution. J Cell Biol 143, 1947–1960.
Lippincott J, Shannon KB, Shou W, Deshaies RJ, Li R (2001). The Tem1 small GTPase controls actomyosin and septin dynamics during cytokinesis. J Cell Sci 114, 1379–1386.
Longtine MS, McKenzie A III, DeMarini DJ, Shah NG, Wach A, Brachat A, Philippsen P, Pringle JR (1998). Additional modules for versatile and economical PCR-based gene deletion and modification in *Saccharomyces cerevisiae*. Yeast 14, 953–961.
Luo J, Vallen EA, Dravis C, Tcheperegine SE, Drees BL, Bi E (2004). Identification and functional analysis of the essential and regulatory light chains of the only type II myosin Myo1p in *Saccharomyces cerevisiae*. J Cell Biol 165, 843–855.
Madania A, Dumoulin P, Grava S, Kitamoto H, Scharer-Brodbeck C, Soulard A, Moreau V, Winsor B (1999). The *Saccharomyces cerevisiae* homologue of human Wiskott-Aldrich syndrome protein Las17p interacts with the Arp2/3 complex. Mol Biol Cell 10, 3521–3538.
McMurray MA, Bertin A, Garcia G 3rd, Lam L, Nogales E, Thorner J (2011). Septin filament formation is essential in budding yeast. Dev Cell 20, 540–549.
McMurray MA, Thorner J (2009). Septins: molecular partitioning and the generation of cellular asymmetry. Cell Div 4, 18.
Meitinger F, Boehm ME, Hofmann A, Hub B, Zentgraf H, Lehmann WD, Pereira G (2011). Phosphorylation-dependent regulation of the F-BAR protein Hof1 during cytokinesis. Genes Dev 25, 875–888.
Meitinger F, Palani S, Hub B, Pereira G (2013). Dual function of the NDR-kinase Dbf2 in the regulation of the F-BAR protein Hof1 during cytokinesis. Mol Biol Cell 24, 1290–1304.
Meitinger F, Petrova B, Mancini Lombardi I, Bertazzi DT, Hub B, Zentgraf H, Pereira G (2010). Targeted localization of Inn1, Cyk3 and Chs2 by the mitotic-exit network regulates cytokinesis in budding yeast. J Cell Sci 123, 1851–1861.
Munn AL, Stevenson BJ, Geli MI, Riezman H (1995). end5, end6, and end7: mutations that cause actin delocalization and block the internalization step of endocytosis in *Saccharomyces cerevisiae*. Mol Biol Cell 6, 1721–1742.
Nishihama R *et al*. (2009). Role of Inn1 and its interactions with Hof1 and Cyk3 in promoting cleavage furrow and septum formation in *S. cerevisiae*. J Cell Biol 185, 995–1012.
Oh Y, Bi E (2011). Septin structure and function in yeast and beyond. Trends Cell Biol 21, 141–148.
Oh Y, Chang K-J, Orlean P, Wloka C, Deshaies R, Bi E (2012). Mitotic exit kinase Dbf2 directly phosphorylates chitin synthase Chs2 to regulate cytokinesis in budding yeast. Mol Biol Cell 23, 2445–2456.
Pollard TD ((2010). Mechanics of cytokinesis in eukaryotes. Curr Opin Cell Biol 22, 50–56.
Ren G, Wang J, Brinkworth R, Winsor B, Kobe B, Munn AL (2005). Verprolin cytokinesis function mediated by the Hof one trap domain. Traffic 6, 575–593.
Roberts-Galbraith RH, Chen JS, Wang J, Gould KL (2009). The SH3 domains of two PCH family members cooperate in assembly of the *Schizosaccharomyces pombe* contractile ring. J Cell Biol 184, 113–127.
Roberts-Galbraith RH, Gould KL (2010). Setting the F-BAR: functions and regulation of the F-BAR protein family. Cell Cycle 9, 4091–4097.
Roberts-Galbraith RH, Ohi MD, Ballif BA, Chen JS, McLeod I, McDonald WH, Gygi SP, Yates JR 3rd, Gould KL (2010). Dephosphorylation of F-BAR protein Cdc15 modulates its conformation and stimulates its scaffolding activity at the cell division site. Mol Cell 39, 86–99.
Rodriguez JR, Paterson BM (1990). Yeast myosin heavy chain mutant: maintenance of the cell type specific budding pattern and the normal deposition of chitin and cell wall components requires an intact myosin heavy chain gene. Cell Motil Cytoskeleton 17, 301–308.
Sanchez-Diaz A, Marchesi V, Murray S, Jones R, Pereira G, Edmondson R, Allen T, Labib K (2008). Inn1 couples contraction of the actomyosin ring to membrane ingression during cytokinesis in budding yeast. Nat Cell Biol 10, 395–406.
Schmidt M, Bowers B, Varma A, Roh D-H, Cabib E (2002). In budding yeast, contraction of the actomyosin ring and formation of the primary septum at cytokinesis depend on each other. J Cell Sci 115, 293–302.
Shannon KB, Li R (2000). A myosin light chain mediates the localization of the budding yeast IQGAP-like protein during contractile ring formation. Curr Biol 10, 727–730.
Shimada A *et al*. (2007). Curved EFC/F-BAR-domain dimers are joined end to end into a filament for membrane invagination in endocytosis. Cell 129, 761–772.
Sikorski RS, Hieter P (1989). A system of shuttle vectors and yeast host strains designed for efficient manipulation of DNA in *Saccharomyces cerevisiae*. Genetics 122, 19–27.
Spencer S, Dowbenko D, Cheng J, Li W, Brush J, Utzig S, Simanis V, Lasky LA (1997). PSTPIP: a tyrosine phosphorylated cleavage furrow-associated protein that is a substrate for a PEST tyrosine phosphatase. J Cell Biol 138, 845–860.
Stevens RC, Davis TN (1998). Mlc1p is a light chain for the unconventional myosin Myo2p in *Saccharomyces cerevisiae*. J Cell Biol 142, 711–722.
Suetsugu S, Toyooka K, Senju Y (2010). Subcellular membrane curvature mediated by the BAR domain superfamily proteins. Semin Cell Dev Biol 21, 340–349.
Sung MK, Huh WK (2007). Bimolecular fluorescence complementation analysis system for in vivo detection of protein-protein interaction in *Saccharomyces cerevisiae*. Yeast 24, 767–775.
Teh EM, Chai CC, Yeong FM (2009). Retention of Chs2p in the ER requires N-terminal CDK1-phosphorylation sites. Cell Cycle 8, 2964–2974.
Tsujita K, Suetsugu S, Sasaki N, Furutani M, Oikawa T, Takenawa T (2006). Coordination between the actin cytoskeleton and membrane deformation by a novel membrane tubulation domain of PCH proteins is involved in endocytosis. J Cell Biol 172, 269–279.
Tully GH, Nishihama R, Pringle JR, Morgan DO (2009). The anaphase-promoting complex promotes actomyosin-ring disassembly during cytokinesis in yeast. Mol Biol Cell 20, 1201–1212.
Vallen EA, Caviston J, Bi E (2000). Roles of Hof1p, Bni1p, Bnr1p, and Myo1p in cytokinesis in *Saccharomyces cerevisiae*. Mol Biol Cell 11, 593–611.
VerPlank L, Li R (2005). Cell cycle-regulated trafficking of Chs2 controls actomyosin ring stability during cytokinesis. Mol Biol Cell 16, 2529–2543.
Versele M, Gullbrand B, Shulewitz MJ, Cid VJ, Bahmanyar S, Chen RE, Barth P, Alber T, Thorner J (2004). Protein-protein interactions governing septin heteropentamer assembly and septin filament organization in *Saccharomyces cerevisiae*. Mol Biol Cell 15, 4568–4583.
Watts FZ, Shiels G, Orr E (1987). The yeast *MYO1* gene encoding a myosin-like protein required for cell division. EMBO J 6, 3499–3505.
Weirich CS, Erzberger JP, Barral Y (2008). The septin family of GTPases: architecture and dynamics. Nat Rev Mol Cell Biol 9, 478–489.
Wloka C, Bi E (2012). Mechanisms of cytokinesis in budding yeast. Cytoskeleton (Hoboken) 69, 710–726.
Wloka C, Nishihama R, Onishi M, Oh Y, Hanna J, Pringle JR, Krauss M, Bi E (2011). Evidence that a septin diffusion barrier is dispensable for cytokinesis in budding yeast. Biol Chem 392, 813–829.
Wloka C, Vallen EA, Thé L, Fang X, Oh Y, Bi E (2013). Immobile myosin-II plays a scaffolding role during cytokinesis in budding yeast. J Cell Biol 200, 271–286.
Wu Y, Spencer SD, Lasky LA (1998). Tyrosine phosphorylation regulates the SH3-mediated binding of the Wiskott-Aldrich syndrome protein to PSTPIP, a cytoskeletal-associated protein. J Biol Chem 273, 5765–5770.
Zhang G, Kashimshetty R, Ng KE, Tan HB, Yeong FM (2006). Exit from mitosis triggers Chs2p transport from the endoplasmic reticulum to mother-daughter neck via the secretory pathway in budding yeast. J Cell Biol 174, 207–220.